Pooled screening identifies combinatorial CAR signaling domains for next-generation CAR-M immunotherapies

Yuxin Wang[1#], Shiman Zuo[1#], Hanjing Bao[1], Zehui Zhang[1], Yijun Chen[2], Wenlong Zhang[2], Qi Liu[1], Yan Lu[1], Yahong Huang[1], Wei Zheng[1], Nanfei Yang[1], Lupeng Ye[3], Pingping Shen[1,2,4*]

[1]State Key Laboratory of Pharmaceutical Biotechnology and Department of Urology, Nanjing Drum Tower Hospital, The Affiliated Hospital of Nanjing University Medical School, School of Life Sciences, Nanjing University, Nanjing 210023, China.

[2]Macera Therapeutics, Nanjing 210032, China.

[3]Institute of Modern Biology, Nanjing University, Nanjing 210023, China.

[4]Shenzhen Research Institute of Nanjing University, Shenzhen 518000, China.

# Equally Contributing Authors.

* Corresponding author.

E-mail address: ppshen@nju.edu.cn (P. Shen)

Abstract

Chimeric antigen receptor-engineered macrophages (CAR-Ms) hold great promise for solid tumor immunotherapy. The intracellular domains (ICDs) of CARs determine the phenotypic output of therapeutic macrophages but remain largely unexplored. Here, we constructed a CAR library containing 131 unique signaling domains derived from native immune receptors and identified 17 ICDs that enhance macrophage phagocytosis, inflammatory responses, or tumor infiltration *in vitro* and *in vivo*. We further developed a scalable 3' barcode technology, CARode, to uniquely label and trace ICD variants within large-scale combinatorial CAR library and applied it to single-cell RNA sequencing and single-cell CAR analysis to assess the synergetic effects of ICD combinations on macrophage activation. Our approach uncovered a novel CD40-LY9-FCRL1 chimeric receptor that modulates the tumor microenvironment and improves solid tumor clearance. In conclusion, our findings demonstrate that pooled screening can accelerate the discovery of complex ICD constructs, providing a powerful platform for engineering macrophage-based immunotherapies.

Introduction

Chimeric antigen receptor T (CAR-T) cell therapy has demonstrated remarkable efficacy in the treatment of hematological malignancies [1, 2]. However, its application in solid tumors has encountered significant challenges, particularly due to limited tumor infiltration and the presence of immunosuppressive tumor microenvironment (TME) [3, 4]. Recently, CAR-engineered macrophages (CAR-Ms) were introduced as an alternative to CAR-T cell therapy for solid tumors [5, 6]. Macrophages have inherent abilities to penetrate solid tumors and modulate the TME through broad immune responses, such as phagocytosis, antigen presentation, and pro-inflammatory cytokine secretion [5, 7, 8]. To harness

this potential, CAR constructs designed to enhance the phagocytic, pro-inflammatory, and tumor-infiltrating functions of macrophages are currently being investigated and have shown promising anti-tumor effects in solid tumors [9-11]. Thus, CAR-engineered macrophages with enhanced anti-tumor functions hold great potential for revolutionizing immunotherapeutic approaches for solid tumors.

The anti-tumor efficacy of CAR-Ms is strongly modulated by the intracellular domains (ICDs) of the CAR constructs [12]. Various engineering strategies have been developed for engineering the signaling domains of CAR-Ms. One current strategy involves tuning CAR signaling via the Fc receptor common gamma chain (FcRγ), which facilitates antibody-dependent cellular phagocytosis (ADCP) [13, 14]. The CD3ζ cytosolic domain, a canonical signaling domain for T cell activation, showed functional similarity with FcRγ signaling in CAR-Ms [10, 15], suggesting the compatibility of receptors that are not typically expressed by macrophages. The second strategy uses Toll-like receptor signaling to drive the M1-like phenotype of therapeutic macrophages [11, 16]. This pro-inflammatory signaling has been combined with the CD3ζ phagocytic domain in CAR-Ms to induce a bifunctional phenotype [11]. Moreover, we previously constructed a CAR bearing the CD147 signaling domain to activate the expression of matrix metalloproteinases (MMPs) to degrade the extracellular matrix (ECM) of solid tumors [9]. Taken together, different ICDs induce distinct phenotypes and functions of therapeutic macrophages. However, the optimal signaling domains required for CAR-M activation and the potential of combinatorial signaling to elicit multifunctional macrophage responses remain largely unexplored.

Advances in large-scale pooled screens, such as genome-wide CRISPR screens and gain-of-function screens, have made it possible to test gene function in a high-throughput manner [17]. Recently, this technology has been applied to CAR engineering, allowing for systematic identification of ICDs, signaling motifs, and transcription factors (TFs) that increase CAR-T cell efficacy [18-22]. However,

such high-throughput approaches have yet to be applied to CAR-M optimization. Several technical challenges hinder the direct application of large-scale CAR screening to macrophage-based therapy. Unlike T cells, primary macrophages exhibit limited proliferative capacity *in vitro* [23], making it difficult to maintain and expand large cell libraries required for pooled screening. Additionally, macrophages have strong antiviral activity [24], which restricts the efficiency of viral-based CAR library delivery. The large size and complexity of CAR libraries further complicate the screening process, as each CAR variant must be effectively expressed and evaluated in parallel. Therefore, novel screening strategies designed for macrophages are required to address current limitations and advance the development of CAR constructs for macrophage-based immunotherapy.

Here, we developed a 131-member natural receptor signaling domain CAR (NaSDC) library to screen the signaling domains of immune response-related receptors as independent ICDs for CAR constructs to promote macrophage activation and anti-tumor functions. The library was screened in the human monocytic cell line THP-1 and validated in human monocyte-derived macrophages (hMDMs). We revealed that 17 ICDs have distinct anti-tumor functions, including phagocytosis, pro-inflammation, and tumor infiltration. Furthermore, we developed a large-scale combinatorial signaling domain CAR (CoSDC) library to evaluate the synergistic effects of signaling combinations of the 17 ICDs in promoting macrophage activation. The CoSDC library was constructed and barcoded via the CARode (Barcode for CAR) strategy, which facilitates unique labels of combinatorial CAR constructs in a scalable manner and is compatible with single-cell RNA sequencing (scRNA-seq). The CoSDC library screens revealed multi-CAR constructs that improved macrophage anti-tumor functions, including a CD40-LY9-FCRL1 chimeric receptor that modulated the TME and improved solid tumor clearance. Overall, these studies highlight NaSDC×CoSDC screening as a powerful method to accelerate the programming of the

macrophage phenotype with enhanced anti-tumor functions.

Results

Design of CAR libraries for CAR-M screens

Here, we aimed to develop a platform that is suitable for high-throughput, pooled screening of CAR signaling domains within macrophages. We developed two libraries to reprogram macrophage function through single ICD CAR overexpression or combined ICD signaling (Figure 1A). The single ICD CAR library aims to assess the role of intracellular elements of natural receptors as independent signaling domains of CAR constructs in promoting macrophage functions, including phagocytosis, tumor infiltration, and pro-inflammatory responses. The combinatorial signaling domain CAR library is designed to evaluate the synergetic effects of ICD combinations on macrophage activation.

Human primary macrophages are resistant to virus-based gene transduction, thus we first needed to determine the proper cell types for large-scale CAR variant screens. The human monocytic cell line THP-1 can be differentiated into macrophages, and this approach has been used previously for genome-wide screening [25, 26]. The infectivity of lentivirus was greater in THP-1 cells than in human monocyte-derived macrophages (hMDMs) (Figure 1B). We confirmed that THP-1-derived macrophages expressed macrophage markers (Figure S1A) and showed the capacity to polarize to the M1, M2 and tumor-associated macrophage (TAM) phenotypes (Figure S1B-S1D). We then transduced CAR variants with the ICD of CD247 (CAR-3ζ) or TLR4 (CAR-t4) into THP-1 cells and observed increased phagocytosis and pro-inflammatory gene expression in THP-1-derived macrophages in response to CAR signaling (Figure S1E-S1I), suggesting that THP-1-derived macrophages constitute a proper model for CAR signaling screening studies.

111 To construct a library for the functional evaluation of natural receptor signaling domains as
112 independent ICDs of CAR constructs within macrophages, we mined macrophage activation-related
113 receptors from various protein families, such as Fc receptors, Toll-like receptors (TLRs), and the TNF
114 receptor superfamily (Figure 1A). Given the homology of receptors across the immune system and the
115 established role of the T cell-related receptor CD3ζ (encoded by *CD247*) as a functional cytosolic domain
116 of CAR-Ms [10], we included receptors that are predominantly expressed in T cells, natural killer (NK)
117 cells, dendritic cells (DCs), and B cells to determine whether subsets of these could engage in distinct
118 and beneficial signaling in macrophages (Figure S2A). Taken together, a total of 131 signaling domains
119 (Table S2) were collected and constructed within the context of a PSMA CAR (containing an anti-PSMA
120 single-chain variable fragment, a CD8α hinge, and a CD8α transmembrane domain) (Figure S2B). The
121 generated library is called the NaSDC library. A truncated CAR without a signaling domain was added
122 to the library as a control. Each CAR variant was uniquely barcoded (Figure S2B) and sequenced to
123 confirm the construct. We then generated NaSDC lentiviruses from the plasmid library to transduce THP-
124 1 cells at a multiplicity of infection (MOI) of 0.3 to minimize multiple integrations per cell (Figure S2C).
125 The ability of NaSDC CAR-Ms to bind to soluble PSMA antigen was confirmed by flow cytometry
126 (Figure 1C). We observed no significant correlation between ICD length and abundance in the CAR-M
127 library (Figure S2D). Together, the NaSDC library provides a robust platform for systematically
128 screening diverse natural receptor signaling domains as independent ICDs of CAR-Ms.

129 We next sought to construct a large-scale combinatorial signaling domain CAR (CoSDC) library to
130 evaluate the synergistic effects of ICD combinations in promoting macrophage activation. A well-
131 established method for identifying different gene variants in large-scale libraries is to use randomized
132 5~20 bp barcode sequences attached to untranslated regions (UTRs) [18, 27, 28], which require pooled

133 PCR and long-read sequencing to match the barcode sequences with gene variants. Here, we developed
134 a novel, scalable method to barcode large-scale CAR libraries, namely CARode (Barcode for CAR).
135 Briefly, we generated constructs with a cloning cassette that was placed between the ICD sequences and
136 barcode sequences (Figure 1D and S3A). The cassette consisted of customized cleavage sites and a stop
137 codon and was flanked by linkers that served as homology arms for assembly (Figure S3B). Each ICD
138 was PCR amplified to combine with the cloning cassette and a unique 6-bp barcode and then incorporated
139 into a PSMA CAR chassis to generate a single ICD CAR (G1) library (Figure S3A). The "2nd ICD-
140 cassette-barcode" constructs were subsequently incorporated into the G1 library to replace the cassette
141 of the first ICD, resulting in a second-generation (G2) CAR library with two fused barcodes (Figure
142 S3A). The third-generation (G3) CARs were generated in a similar way (Figure S3A). This approach
143 could theoretically enable more than 16 million possible combinatorial CARodes for the G2 library and
144 over 68 billion CARodes for G3 CARs. Given their proximity to the 3' UTR, these tandem CARodes
145 allow sequencing of CAR identities in single-cell transcriptomes using commercially available 3' capture
146 kits (Figure 1D). Additionally, the arrangement of CARodes reflect the order of ICDs in CAR constructs,
147 and the length of CARodes indicates the generation of CARs (Figure 1D). In summary, CoSDC screens
148 with CARode technology enable rapid evaluation of CAR ICD combinations for engineered
149 immunotherapies.

150 **NaSDC allows for the discovery of CAR-M variants with distinct anti-tumor functions**

151 We first aimed to identify signaling domains that trigger the phagocytosis of macrophages in the context
152 of CARs. We adopted a bead-based selection strategy for the rapid separation of CAR-Ms on the basis
153 of their ability to phagocytose magnetic substrates (Figure 2A). After incubation with magnetic particles,
154 NaSDC library cells were passed through a uniform magnetic field that selectively captured magnetized

155 cells that had ingested magnetic particles, while cells that did not phagocytose beads passed through.
156 Subsequently, RNA was isolated and reverse transcribed into cDNA, followed by barcode sequencing to
157 compare the abundance of each CAR variant in the input and output populations.

158 We integrated beta scores from the robust rank aggregation (RRA) model with overall fold changes
159 to evaluate CAR enrichment in the output populations. The screening was performed in sextuplicate to
160 enable RRA model and reduce batch effects. The results of the two algorithms were strongly correlated
161 (Figure 2B). Notably, we found that the previously reported pro-phagocytic signaling domains FCER1G
162 and CD247 were highly enriched in the output pools (Figure S4A). Signaling by Fc receptor superfamily
163 had strong effects on macrophage phagocytosis, especially FCRL1 and FCRL6, which exhibited similar
164 pro-phagocytosis capacity compared with FCER1G signaling (Figure S4B). Among the top positive hits
165 were HCST (encoding DAP10), which is required for NK cell activation and associated with T cell
166 responses [29], and TREML1, which can promote the aggregation of platelets [30] (Figure 2B).
167 Interestingly, the inhibitory signals BTLA and LILRB2, which are expressed primarily in T cells and NK
168 cells [31, 32] (Figure 2B), also promote macrophage phagocytosis, suggesting distinct functions of these
169 receptors in macrophages. Overall, eight signaling domains showed an enhanced ability to phagocytose
170 magnetic substrates compared with FCER1G signaling.

171 We next sought to validate the pro-phagocytic function of the CAR variants in human primary
172 macrophages. Given that macrophages are antiviral-transfected cells, we adopted a lipid nanoparticle
173 (LNP) delivery system to transfer CAR-encoded mRNAs into primary human macrophages. LNPs
174 exhibited high gene transduction efficiency and fast protein expression in the context of primary
175 macrophages (Figure S5A and S5C). The expression level peaked at 12 hours post-transfection and
176 remained stable for up to 10 days in the cells (Figure S5A). We transduced the mRNAs of the pro-

177 phagocytic CARs into hMDMs and confirmed their phagocytosis of the antigen-positive tumor cells
178 (Figure 2C). Notably, all ICD variants exhibited higher pro-phagocytic capacity compared with CAR-
179 FCER1G (Figure 2C). Among these variants, the CAR-FCRL6 and CAR-FCRL1 variants exhibited the
180 best performance (Figure 2C).

181 Therapeutic macrophages must maintain a persistent pro-inflammatory phenotype within tumors to
182 support their anti-tumor functions [7]. However, macrophages are plastic cells and can shift to an
183 immunosuppressive phenotype in response to TME signals [7, 8]. To explore CAR variants that can
184 repolarize immunosuppressive TAMs to a pro-inflammatory phenotype, we performed NFκB pathway
185 activity screens using an iRFP670 fluorescent reporter (Figure 2D). The reporter was cotransduced with
186 the NaSDC library into THP-1 cells to generate a reporter CAR-M library. We pretreated the reporter
187 cells with conditioned media from prostate cancer cell cultures for two days to mimic the
188 immunosuppressive TME. Downregulation of iRFP fluorescence induced by tumor media was observed
189 (Figure S4C). The CAR-Ms were subsequently cocultured with antigen-positive target cell lines, and
190 iRFP670^{high} cells were sorted (Figure S4D) and subjected to barcode sequencing.

191 Polarization screening revealed eight signaling domains with notable impacts on macrophage pro-
192 inflammatory polarization (Figure 2E and S4E). We noted that both the TNF receptor superfamily and
193 TLR family signals promoted NFκB activation (Figure S4F), whereas chimeric receptors with TNF
194 superfamily intracellular domains, such as CD40, LTBR, TNFRSF1A, and TNFRSF11A, tended to
195 perform better in this context (Figure 2E). The transduction of TNFRSF1A-CARs and LTBR-CARs into
196 hMDMs resulted in limited surface expression and decreased cell viability even in the absence of
197 stimulation (Figure S5B and S5D), suggesting potential stimulation-independent effects. Validation
198 analyses revealed that the top variants can increase the pro-inflammatory phenotype and cytokine

199 secretion (Figure 2F and S6A-S6C).

200 To discover CAR signaling that can promote macrophage infiltration, we next screened the NaSDC
201 pool in a subcutaneous tumor model (Figure 2G). We subcutaneously (SC) injected PSMA-positive
202 prostate tumors and peritumorally injected NaSDC macrophages 7 days after tumor inoculation. Four
203 days later, the tumors were harvested, and the abundance of barcodes was measured using barcode
204 sequencing (Figure S7A). We computed CAR variant enrichment as described above and merged the
205 results from all of the mice. We observed high enrichment of CAR-Ms with LY9 and CD247 ICDs in the
206 tumor tissues (Figure 2H and S4G). The potential of LY9 and CD247 signaling to increase macrophage
207 abundance in solid tumors was validated in an independent assay in which hMDMs bearing either CAR-
208 LY9 or CAR-3ζ were injected around the tumor sites, and both of these CAR-Ms were significantly
209 enriched in target-positive tumors (Figure S7B). Validation analyses revealed that MMP family gene
210 expression levels increased in these CAR-Ms during coculture with antigen-positive cells (Figure 2I,
211 S5E, and S7C-S7E), suggesting enhanced matrix degradation capacity. We noted that these CAR variants
212 lack the ability to induce a pro-inflammatory response in macrophages (Figure S7D and S7E). RNA-seq
213 analysis revealed a transcriptional similarity of 46% in upregulated genes between LY9 and CD247 CAR-
214 Ms (Figure S7F). Biological process analysis showed that CAR-LY9 and CAR-3ζ macrophages behaved
215 more similarly in terms of cell proliferation (Figure S7G).

216 In summary, we identified 17 signaling domains, including two previously reported ICDs (FCER1G
217 and CD247), that can elicit pro-phagocytic, pro-inflammatory, or pro-infiltrating functions in
218 macrophages through NaSDC screens. These functional signaling domains hold potential for guiding the
219 design of combinatorial signaling domain CARs that benefit to macrophage-based therapies.

220 **CoSDC enables pooled screening of ICD combinations via scRNA-seq and scCAR-seq**

221 We next explored ICD combinations that could trigger combinatorial functions of macrophages via the
222 CoSDC library. To construct the CoSDC library, we randomly integrated the 17 ICDs identified from
223 NaSDC screens to generate second- and third-generation CAR constructs, yielding a theoretical diversity
224 of 5219 barcoded signaling domain combinations. As described above, each signaling domain receives
225 a unique barcode sequence to de-multiplex CAR generation, ICD type and position. Barcode sequencing
226 revealed that the CoSDC plasmid library possessed all possible combinations, with balanced
227 representation (Figure S8A). We then generated lentiviruses to transduce THP-1 cells at a low MOI to
228 minimize multiple integrations per cell (Figure S8B). The CAR-M library was PMA-stimulated and
229 cocultured with antigen-positive target cells. Macrophages bearing truncated CARs were incorporated
230 into the pooled cocultures as negative controls. Following 24 h of coculture, CAR-Ms were isolated by
231 FACS (Figure S8C) and processed for scRNA-seq through the 10X Genomics pipeline (Figure 3A).
232 Barcoded CAR transcripts found in the scRNA-seq cDNA product were selectively amplified and
233 sequenced.

234 The transcriptomes of 13,471 CAR-Ms were obtained from scRNA-seq following data
235 preprocessing and filtering (Figure 3B). Among these cells, 58.7% could be assigned a single specific
236 CAR variant (Figure 3B), while the remaining cells were excluded because of either the absence of CAR
237 insertion or the presence of multiple distinct CAR constructs within the same cell. Interestingly, we noted
238 that CAR variants triggered different functional macrophage states upon encountering target cells. Seven
239 clusters were identified using unsupervised clustering (Figure 3B). Cluster c6 exhibited a combinatorial
240 phenotype characterized by M2-like polarization (Figure 3C) and MHC I-mediated antigen processing
241 and presentation (Figure 3D and S9A). Cluster c5 displayed a similar polarization pattern to that of c6
242 but higher levels of MMP expression (Figure 3C and 3E). Both clusters c0 and c3 significantly

243 upregulated the expression of MMP (Figure 3E) and phagocytosis-related genes (Figure 3F), but c3 failed
244 to transition into an M1-like phenotype (Figure 3C) and had diminished antigen processing and
245 presentation ability (Figure 3D and S9A). Notably, CAR-Ms in cluster c0 exhibited M1-like polarization,
246 antigen processing and presentation, MMP expression, and phagocytosis (Figure 3C-F and S9A-C),
247 suggesting that the signaling domains within c0 CARs can trigger combinatorial anti-tumor functions of
248 macrophages.

249 We next tracked the extent of enrichment for each ICD at each position in the c0 cluster. Consistent
250 with the standard second- and third-generation of CAR-T cell constructs [1, 33], the CD247 signaling
251 domain tended to perform better at the C-terminal end of the CAR-M constructs (Figure 3G). In contrast,
252 some ICDs (e.g., TNFRSF1A and LTBR) are suitable for grafting into the membrane-proximal
253 intracellular space of a CAR (Figure 3G). HCST, TYROBP, and LY9 signaling can be incorporated into
254 any of the three intracellular positions in a third-generation CAR construct (Figure 3G). These results
255 demonstrate the positional preferences of different ICDs when incorporated into a combinatorial
256 signaling CAR.

257 **CoSDC library-guided CAR constructs induce a favorable macrophage phenotype**

258 To validate the CoSDC-guided CAR variants and understand their effects on macrophage activation and
259 anti-tumor functions, we selected and cloned eight CAR variants from the CoSDC library, based on the
260 ICD features of cluster c0 (Figure 4A). Each variant consists of a pro-phagocytic module, a pro-
261 inflammatory module, and a pro-infiltrating module. The ability of CAR-M variants to bind to PSMA
262 antigen was confirmed by flow cytometry (Figure S10A). The ICD sizes ranged from ~1,000–2,000 bps,
263 and little correlation was observed between the ICD size and surface expression efficiency (Figure S10B
264 and S10C). Interestingly, we observed significantly different CAR surface expression levels between

265 constructs with the same ICD elements but different arrangements (COMB1: HCST-LY9-TNFRSF11A,
266 and COMB4: TNFRSF11A-HCST-LY9) or constructs containing one different ICD (COMB2: LY9-
267 FCER1G-CD247, and COMB3: LY9-FCER1G-KIR2DS1) (Figure S10D and S10E), suggesting that the
268 ICD type and position modulate CAR surface expression within macrophages.

269 We next evaluated the effect of the combinatorial signaling of CARs on macrophage activation. We
270 incubated CAR-Ms with mTagBFP2-expressing PC3-PSMA cells at an effector/target (E/T) ratio of 1/1
271 and observed that COMB3, COMB6, COMB7 and COMB8 CARs led to remarkable phagocytosis of
272 tumor cells compared to UTD cells over a time course of 4 hours (Figure 4B). Among these CAR-Ms,
273 COMB6 and COMB7 CAR-Ms showed the best performance in promoting phagocytosis, suggesting
274 their anti-tumor activity *in vitro*. We noted that all eight CAR variants presented high CD80 and CD86
275 expression (Figure 4C). Consistent with these findings, the reactive oxygen species (ROS) levels (Figure
276 4D) and the *IL6* and *TNF* expression levels were increased in these CAR-Ms (Figure 4E), suggesting
277 their pro-inflammatory ability. In addition, we noted that all the CAR variants except COMB5 promoted
278 MMP family gene expression in macrophages (Figure 4F). In summary, the NaSDC and CoSDC libraries
279 facilitated the rapid identification of CAR ICD combinations that exhibit synergetic anti-tumor effects in
280 CAR-M immunotherapy. We chose the COMB7 CAR construct for further development due to its robust
281 pro-phagocytic function and comparable pro-inflammatory and pro-infiltrating capabilities.

282 **A novel CD40-LY9-FCRL1 CAR-M modifies the TME**

283 Given that the COMB7 construct promoted pro-inflammatory phenotypes of macrophages *in vitro,* we
284 evaluated the interactions of COMB7 CAR-Ms within the TME in a humanized immune system mouse
285 model (Figure 5A). Given the variability in the immune system reconstitution rates among individuals,
286 we adopted a bilateral tumor model to ensure comparability between groups. Briefly, PSMA-positive

287 prostate tumors were bilaterally inoculated into the subcutaneous flanks of NCG mice. After confirmation
288 of tumor engraftment, human peripheral blood mononuclear cells (PBMCs) were transplanted to
289 reconstitute the immune system. UTD or COMB7 CAR-Ms were injected intratumorally (IT) into either
290 the right or left flank. Four days later, the tumors were harvested, and the CAR expression levels were
291 measured in matched tumor tissues (Figure S11A). The human CD45-positive cells were sorted and
292 subjected to scRNA-seq (Figure S11B). The transcriptomes of 17,432 individual cells were obtained
293 from scRNA-seq following data filtering, of which 44.6% were macrophages and 40.4% were identified
294 as T cells (Figure 5B and S11C).

295 Using the scRNA-seq data, we analyzed the phenotypic and functional changes of macrophages in
296 the TME caused by COMB7 CAR-M treatment. We isolated CAR-positive macrophages (Figure 5C and
297 5D) from COMB7 CAR-M-treated tumors and observed a strong M1-like polarization phenotype in these
298 cells (Figure 5E). Notably, CAR-negative macrophages from the COMB7 flank group presented higher
299 levels of M1 features than those from the UTD group (Figure 5E and 5F), suggesting that COMB7 CAR-
300 Ms can maintain a pro-inflammatory microenvironment within the human TME. Although macrophages
301 from UTD-treated tumors expressed several M1-related genes, such as *IL1B* and *IL6*, these cells
302 simultaneously expressed the M2 markers CD163 and MRC1 (CD206) (Figure 5E and 5F). Consistent
303 with these findings, UTD cells upregulated the expression of anti-inflammatory cytokines such as IL-10,
304 which promote an immunosuppressive TME (Figure S11D). In addition, macrophages from the COMB7
305 flanks exhibited higher levels of MMP9, suggesting increased ECM degradation capacity (Figure S11D).
306 Together, these data demonstrate that COMB7 CAR-Ms have the ability to reduce tumor-induced M2
307 polarization and maintain an inflammatory TME in solid tumors.

308 The immunosuppressive environment of solid tumors can drive exhaustion and dysfunction of T

309 cells [34, 35]. Given the improved TME caused by COMB7 CAR-M treatment and the upregulation of
310 costimulatory ligands as well as antigen processing and presentation genes in macrophages (Figure 5F
311 and 5G), we examined whether COMB7 CAR-M therapy could change T cell behavior in solid tumors.
312 We observed no significant correlations between cytotoxicity scores and COMB7 CAR-M treatment, but
313 the exhaustion scores were notably decreased in the $CD8^+$ T cells of the COMB7 group (Figure 5H).
314 These data suggest that COMB7 CAR-M treatment maintains T cell function in solid tumors.

315 **CD40-LY9-FCRL1 CAR improves solid tumor clearance**

316 We next evaluated the *in vitro* killing capacity of the COMB7 CAR-induced macrophages. The COMB7
317 CARs were transduced to hMDMs using the LNP method. No correlation was observed between the
318 intracellular levels of CAR-encoded mRNA and the killing efficacy (Figure S12A). We cocultured
319 $PSMA^+$ cancer cells with COMB7 CAR-Ms and observed that the COMB7 CAR improved the killing
320 capacity across multiple E/T ratios (Figure 6A). Notably, UTD macrophages had a strong tumor killing
321 effect at an E/T ratio of 10/1 (Figure 6A), suggesting the intrinsic anti-tumor function of primary
322 macrophages. Compared with the CAR-3ζ, the COMB7 CAR showed increased cytotoxicity in
323 macrophages from two human donors (Figure 6B). We next evaluated the killing capacity of the COMB7
324 CARs in different tumor models. We generated COMB7 CAR-Ms targeting the solid tumor antigens
325 HER2 or GPC3 and cocultured these CAR-Ms with antigen-positive tumor cells. We observed significant
326 killing of HER2-positive SKOV3 cells in COMB7 CAR-M cocultures (Figure 6C). Both UTD- and
327 COMB7-engineered macrophages exhibited high killing capacity in GPC3-positive HepG2 cells (Figure
328 6D).

329 We next evaluated the *in vivo* killing capacity of COMB7 CAR-Ms in NCG mice that were
330 challenged with intraperitoneal (IP) prostate tumors (Figure 6E). The mice were treated one day later

331 with a single IP injection of PBS, UTD macrophages or anti-PSMA CAR-Ms. Animal imaging was
332 conducted to monitor tumor growth. Compared with those in the control groups, macrophages engineered
333 with COMB7 CAR enhanced tumor control and survival (Figure 6F, 6G and S12B). In summary, these
334 data demonstrate that COMB7-based CARs can direct tumor killing activity and provide support for
335 subsequent efforts to translate this platform to the clinic.
336

337 **Discussion**

338 The signaling domains of CAR constructs strongly modulate the phenotypic output of CAR-Ms. To
339 discover ICDs that can enhance CAR-M anti-tumor functions, we designed a two-step NaSDC×CoSDC
340 screening platform. The NaSDC library contains CARs with single ICDs derived from immune response-
341 related receptors. NaSDC screening allows us to filter out ICDs with weak anti-tumor effects. CAR
342 variants with different anti-tumor potentials were selected from NaSDC and randomly combined to
343 generate CoSDC. We integrated CoSDC library with scRNA-seq and scCAR-seq to identify synergistic
344 ICD combinations that enhance macrophage anti-tumor functions. As a result, NaSDC screening
345 identified 17 functional CARs with previously unused intracellular signaling domains. Subsequent
346 CoSDC screening using the random combinations of these 17 ICDs identified a novel CD40-LY9-FCRL1
347 CAR construct with enhanced anti-tumor functions. Together, the CAR candidates identified by the
348 screening platform exhibit functions that are uncommon in current CAR-M designs and may lead to new
349 applications for effective CAR-M therapies.

350 Unbiased combinatorial CAR signaling domain screens now serve as powerful tools for identifying
351 candidates for improving T cell differentiation, activation, and cytotoxicity in CAR-T therapy [18-20,
352 22]. However, this screening strategy has not been applied to optimize CAR macrophages. Previous

353 studies have focused primarily on designing CAR-Ms on the basis of known activation and polarization
354 mechanisms of macrophages. Given the conservation of receptor signaling pathways across the immune
355 system [36-38], we hypothesized that certain receptors, which are not naturally expressed in
356 macrophages, could nevertheless activate these cells when incorporated into a CAR construct. Indeed,
357 previous studies have reported T cell-related receptor CD3ζ as a phagocytic domain of CAR-Ms [10, 15].
358 Our NaSDC screens demonstrate that lymphatic receptors such as CD3E and ICOS can function as
359 intracellular signaling domains to promote inflammatory responses or enhance phagocytosis in
360 macrophages. Together, these results extend the range of signaling domains from other cell types that
361 can act upon macrophages. Furthermore, macrophages exhibit a wide range of activation states upon
362 sensing and responding to combined cues in their microenvironment [39-41], which cannot be accurately
363 predicted at present. Using the CoSDC platform in combination with scRNA-seq and scCAR-seq, we
364 found that the combinatorial signaling induced at least seven distinct macrophage activation states,
365 although many of the CAR signaling domains have similar activation mechanisms or functions. These
366 findings underscore the unpredictable nature of macrophage activation in response to combinatorial
367 signaling, highlighting the critical importance of pooled screening strategies in advancing macrophage-
368 based engineered cell therapies.

369 Gene transduction remains a major challenge in macrophage research. Lentiviral transduction is the
370 primary method for large-scale library delivery. However, macrophages express retroviral restriction
371 factors such as SAMHD1 [42-44], which limit the efficiency of lentiviral-based gene transduction.
372 Previous pooled screening using human monocytic cell line (U937 and THP-1) to overcome these
373 limitations [25, 26, 45]. In our study, we used PMA-differentiated THP-1 cells as an alternative model
374 to conduct NaSDC and CoSDC screening. While this model does not fully replicate the characteristics

375 of activated macrophages [46, 47], we observed similar phenotypic outputs between THP-1-derived
376 macrophages and hMDMs in response to CAR signaling in NaSDC library screens, indicating its
377 reliability for CAR identification. To enable direct screening in human primary macrophages, future
378 research should develop more efficient gene delivery methods, such as improved viral vectors, or non-
379 viral systems, to overcome retroviral restrictions and support CAR-M development.

380 Although we focused on anti-tumor functionality, NaSDC×CoSDC has potential for optimizing
381 CAR-M therapy in various diseases, such as autoimmune diseases, cardiac injuries, and liver fibrosis.
382 These conditions involve distinct macrophage phenotypes with diverse functions, such as anti-
383 inflammatory responses, tissue repair, and fibrosis attenuation. Moving forward, the NaSDC×CoSDC
384 strategy should not be limited to CAR domain screening but should be expanded to include the selection
385 of TF combinations, cytokine combinations, and even random combinations of CARs, TFs and cytokines
386 to further increase macrophage activation and polarization. Moreover, the integration of CoSDC with
387 scRNA-seq can be used not only to find CAR signaling domains but also as an optimal approach for
388 investigating the intricate mechanisms of macrophage polarization, making it possible to obtain
389 snapshots of individual macrophages upon stimulation with different combinations of signals. Together,
390 the NaSDC×CoSDC strategy will accelerate the process of candidate selection and design optimization
391 for combinatorial constructs, advancing the discovery of biological mechanisms and supporting the
392 development of a broad range of cellular therapies.

393

394 **Methods**

395 **Cell lines**

396 HEK293T (referred to as 293T), THP-1, PC-3, K562 cell lines were purchased from the cell bank of the

397 Committee on Type Culture Collection of the Chinese Academy of Sciences. 293T cells were cultured in
398 DMEM. THP-1, PC-3 cells were maintained in RPMI 1640 medium. To obtain macrophages, THP-1
399 cells were differentiated with 1 ng/ml phorbol 12-myristate 13-acetate (PMA) for 48 h. PC-3 cells were
400 transduced with a construct of FFluc-P2A-mTagBFP2 (FFLuc-BFP) to stably express firefly luciferase
401 (FFLuc) along with a mTagBFP2 fluorescence. PC-3-FFLuc-BFP (referred to as PC3) cells were then
402 transduced with lentiviral vectors encoding PSMA (*FOLH1*) to generate PC3-PSMA cells. K562 cells
403 were transduced with lentiviral vectors encoding PSMA to generate K562-PSMA cells. Cells were
404 maintained in culture medium supplemented with 10% fetal bovine serum (FBS, GIBCO) and 1%
405 penicillin/streptomycin at 37 °C with 5% CO_2 in a humidified incubator.
406
407 **Primary cells**
408 De-identified healthy male and female donor blood samples were provided by the SAILYBIO Co., Ltd.
409 Sample acquisitions were approved and regulated by the Shanghai Liquan Hospital Institutional Review
410 Board (XF-WBC-220809). PBMCs were isolated from blood samples by density gradient centrifugation
411 with Lymphocyte separation medium (Yeasen). Monocytes were isolated from PBMCs from all cell
412 sources by positive selection with anti-CD14 magnetic beads (Miltenyi Biotec). For macrophage
413 differentiation, isolated $CD14^+$ monocytes were seeded on plates in X-VIVO 15 medium (Lonza)
414 supplemented with 10% FBS and 50 ng/ml GM-CSF (Yeasen) and cultured for a further 7 days at 37 °C
415 with 5% CO_2.
416
417 **Xenogeneic mouse models**
418 All mouse procedures and experiments for this study were approved by the Institutional Animal Care

419 and Use Committee at Nanjing University (IACUC-2306005). Animals were housed in a temperature-
420 controlled specific pathogen-free facilities with a 12 h light/dark cycle with 45-65% relative humidity.
421 Food and water were available ad libitum. All mice were more than 8 weeks old at the beginning of the
422 experiments. Animal sample sizes were determined based on previous studies and literatures of the field
423 using similar experimental paradigms.

424 Male NOD/ShiLtJGpt-*Prkdc*^{em26Cd52}*Il2rg*^{em26Cd22}/Gpt (NCG) mice were purchased from
425 GemPharmatech. For tumor control and survival analyses, mice were injected IP with 1×10^6 PC3-PSMA
426 cells. 24 hours later, 5×10^6 CAR-Ms, UTD macrophages or PBS were injected IP. Tumor burden was
427 monitored once per week by IP injection of D-Luciferin, Potassium Salt (Yeasen) at a dose of 150 mg/kg,
428 then measurement of bioluminescence with an IVIS Spectrum imaging system (PerkinElmer). Tumor
429 burden was quantified by total photon counts using the LivingImage software. Mice were weighed
430 weekly and were subject to routine veterinary assessment for signs of overt illness. Animals were killed
431 at experimental termination or when predetermined IACUC rodent health endpoints were reached. For
432 TME analyses, 4×10^6 PC3-PSMA tumor cells were resuspended in Ceturegel Matrix LDEV-Free
433 Matrigel (Yeasen) and injected SC into both flanks of NCG mice. After confirmation of tumor
434 engraftment (about seven days), mice were engrafted intravenously (IV) with 2×10^7 human PBMCs. On
435 day 14, 5×10^6 UTD or COMB7 CAR-Ms were injected IT into either the right or left flank. Four days
436 later, the tumors were harvested for further analysis.

437

438 **NaSDC library construction**

439 The lentiviral vector pHIV-EGFP was gifted by Bryan Welm and Zena Werb (Addgene plasmid #21373).
440 To generate a backbone vector for ICD insertion, a codon-optimized gene encoding PSMA CAR

441 composed of CD8α signal peptide, J591 single-chain variable fragments (scFv), CD8α hinge and
442 transmembrane domain was commercially synthesized by GenScript and cloned into the pHIV-EGFP
443 vector. An Esp3I cleavable linker and a randomized 18-nucleotide sequence were insert to C-terminal
444 portion of the CAR construct. The backbone vector was digested with FastDigest Esp3I (Thermo Fisher),
445 and 131 immune response-related ICDs (Table S2) were individually cloned into the vector using Gibson
446 Assembly. Then, the bacterial transformation was conducted using the obtained products, and colonies
447 were randomly selected. Sequences were performed to identify the correct encoding plasmid with a
448 unique barcode for each CAR variant. The single CAR variant plasmids were pooled at equimolar ratios,
449 electroporated into Endura Electrocompetent cells (LGC), and purified to generate the NaSDC plasmid
450 library.
451
452 **Lentiviral library production**
453 The plasmids pMD2.G and psPAX2 were gifts from Didier Trono (Addgene plasmid #12259 and
454 #12260). To produce lentivirus, 293T cells were transfected with a plasmid library and the packaging
455 plasmids psPAX2 and pMD2.G using Lipofectamine 2000 Transfection Reagent (Thermo Fisher) at a
456 mass ratio of 24:3:1. Medium was changed 12 h after transfection, and the supernatant containing
457 lentiviruses were collected in 48-72 h after transfection. The supernatant was filtered through 0.45 μm
458 non-pyrogenic filters. To concentrate lentiviruses, the Lenti-Concentin Virus Precipitation Solution
459 (ExCell Bio) was added to the supernatant for 12, and centrifuged for 30 min at 2,000 × *g*. The pellet
460 was then resuspended in OptiMEM medium (Thermo Fisher) and stored at -80 °C. Medium containing
461 concentrated lentiviral library was used to infect THP-1 cells in the presence of 8 μg/ml polybrene
462 (Yeasen).

463

464 **Pro-phagocytic CAR variant screens**

465 Streptavidin-coated magnetic beads (ACROBiosystems) were sterilized for 30 min in 70% isopropanol.
466 Beads were spun down and resuspended in OptiMEM. Biotinylated human PSMA proteins
467 (ACROBiosystems) were added to the beads at a concentration sufficient to occupy 25% of the binding
468 sites. After incubation for 1 h, the beads were washed using PBS and resuspended in OptiMEM. The
469 PSMA-labeled beads were added to macrophages carrying NaSDC library at a bead-to-cell ratio of 5:1.
470 After phagocytosis for 2 h, cells were rinsed eight times by PBS to remove un-ingested particles. Then,
471 the cells were trypsinized, harvested and sorted using a magnetic holder. The captured cells were washed
472 three times by PBS. The input NaSDC CAR-M library and the magnetic sorted cells were store at -80 °C
473 in TRIzol reagent (Thermo Fisher) for subsequent barcode sequencing.

474

475 **Pro-inflammatory CAR variant screens**

476 To enable screening with fluorescent NFκB reporter system, a construct composed of NFκB response
477 elements (NFRE), a minimal TATA-box promoter, and an iRFP670 fluorescent reporter was cloned into
478 a pLenti6/V5 lentiviral vector to replace the CMV promotor. The fluorescent reporter was then stably co-
479 transduced into THP-1 cells with NaSDC library, and the positive cells were selected using blasticidin
480 (10 μg/ml). The reporter NaSDC THP-1 cells were induced by 1 ng/ml PMA for 48 h. After
481 differentiation, PMA was washed out with PBS, and PC3 conditional media were added to the cells for
482 48 h to induce TAM polarization. The polarized CAR-M pool was cocultured with PC3-PSMA cells at a
483 ratio of 1:1 for 24 h. Following coculture, cells were trypsinized, and resuspended in FACS buffer (PBS
484 + 1-2% FBS), and iRFP670^{high} cells were sorted by a FACSAria II Cell Sorter (BD Biosciences). The

485 input reporter NaSDC CAR-M library and the sorted cells were store at -80 °C in TRIzol reagent (Thermo
486 Fisher) for subsequent barcode sequencing.
487
488 **Pro-infiltrating CAR variant screens**
489 THP-1 cells were lentivirally transduced with a NaSDC library, and the positive cells were selected using
490 flow cytometry. NCG mice were dosed with 2×10^6 PC3-PSMA tumor cells through subcutaneous
491 injection. The NaSDC THP-1 cells were induced by 1 ng/ml PMA for 48 h, and 1×10^7 NaSDC CAR-Ms
492 were peritumorally injected 7 days after tumor inoculation. Four days later, the tumors were harvested.
493 The input NaSDC CAR-M library and the tumor tissues containing infiltrated CAR-Ms were store at -
494 80 °C in TRIzol reagent (Thermo Fisher) for subsequent barcode sequencing.
495
496 **Barcode sequencing and data analysis**
497 RNA was extracted from input and output population using TRIzol reagent, and reversely transcribed
498 into cDNA using HiScript IV 1st Strand cDNA Synthesis Kit (Vazyme). Subsequently, barcode sequences
499 were PCR amplified, and Illumina sequencing adaptors were appended using NEBNext Ultra II Q5
500 Master Mix (NEB). SYBR Green I (MeilunBio) was incorporated to the rection system to monitor the
501 progression of PCR. The cDNA was amplified in a C1000 thermocycler (Bio-Rad) until the fluorescent
502 signal approached the termination of exponential phase. Then, the products were immediately transferred
503 to another thermocycler, and incubated at 72 °C for 5 min to complete the PCR program. The PCR
504 products were bead-purified and sequenced by Novogene on an Illumina NovaSeq X Plus Sequencer.
505 Considering the limited *in vitro* proliferation ability of macrophages, a single round screening would
506 result in an elevated false positive rate within the output populations. Therefore, we repeated the

507 screening experiments and sequencing runs to minimize the experimental bias.

508 DESeq2 (v1.42.1) [48] and RobustRankAggreg (v1.2.1) [49] R packages were integrated to
509 compute the alterations of barcodes in output vs input populations. DESeq2 was used to merge the
510 repeated experiments and calculate the overall log2 fold change (log2FC) of barcode representation. In
511 the RobustRankAggreg analysis, the log2FC was calculated separately for each experimental batch. The
512 barcodes were then ranked based on their log2FC and aggregated using RRA algorithm. RRA method
513 uses rho score to retrieve the positive factors from the noise, and represent the significance probabilities
514 for all the elements. The rho score < 0.05 and overall log2FC > log2FC (CARΔ) was considered as
515 positive enrichment in output population.

516

517 **In vitro mRNA transcription**

518 The genes encoding indicated CAR variants or EGFP control were codon-optimized and cloned into a
519 plasmid carrying a T7 promoter, 5' and 3' UTR elements, and a poly(A) tail. The plasmids were linearized
520 by FastDigest LguI (Thermo Fisher), and the mRNA was synthesized using T7 Co-transcription RNA
521 Synthesis Kit (Syngene). N1-methyl-pseudouridine-5′-triphosphate (N1-Me-pUTP) was substituted for
522 uridine triphosphate. Capping of the IVT mRNAs was performed co-transcriptionally using a
523 trinucleotide cap1 analog CAP GAG (Syngene). The generated mRNAs were purified using VAHTS
524 RNA Clean Beads (Vazyme). All mRNAs were analyzed by agarose gel electrophoresis and stored at -
525 80 °C before uses. 10 pmol mRNAs were used to transduce 1×10^6 hMDMs via Lipofectamine
526 MessengerMAX Transfection Reagent (Thermo Fisher) according to the manufacturer's protocol. The
527 medium was changed 12 h after transduction, and flow cytometry was performed to detect surface
528 expression of CAR proteins.

529

530 **Flow cytometry**

531 To block non-specific bindings, FcR Blocking Reagent (Miltenyi Biotech) was always used for staining
532 of monocytes, macrophages or monocytic cell lines expressing Fc receptors. Macrophage purity was
533 tested using the following antibodies: Anti-human CD11b PE (1:100, BioLegend), Anti-human CD14
534 APC (1:100, BioLegend), Anti-human CD68 APC (1:100, BioLegend). M1 markers on human
535 macrophages were detected with the following antibodies: Anti-human CD80 FITC (1:100, BioLegend),
536 Anti-human CD86 APC (1:100, Thermo Fisher). Surface anti-PSMA CAR expression was detected using
537 PE-Labeled Human PSMA (ACROBiosystems), or Biotinylated Human PSMA (ACROBiosystems)
538 followed by Streptavidin/APC (Solarbio) staining. Flow cytometric analysis was performed on a
539 NovoCyte Flow Cytometer (ACEA Biosciences) or an Attune NxT Flow Cytometer (Thermo Fisher).
540 The data were analyzed by NovoExpress (v1.6.2) and visualized by CNSplot (v1.0.1) R package.

541

542 **Phagocytosis assay**

543 The PC3-PSMA cells were transduced to stably express mTagBFP2 fluorescence as described above.
544 The mTagBFP2 is a blue fluorescent protein with lower sensitivity to the acidic environment of the
545 lysosome compared to other fluorescence proteins such as EGFP [50]. For each CAR variant, 5×10^5 UTD
546 or CAR-Ms were cocultured with 5×10^5 PC3-PSMA cells for 4-6 h at 37 °C. After coculture, cells were
547 harvested with Accutase (Yeasen) and resuspended in FACS buffer. The CAR-Ms were stained with PE-
548 Labeled Human PSMA (ACROBiosystems), and the UTD cells were stained with Anti-human CD11b
549 PE (BioLegend). The cells were analyzed using an Attune NxT Flow Cytometer (Thermo Fisher). The
550 percent of mTagBFP2$^+$ events within the PE$^+$ population was plotted as percentage phagocytosis.

551

552 **Quantitative real-time PCR (qPCR)**

553 Total RNA was isolated from cells or tumor tissue samples with TRIzol reagent. Reverse transcription
554 was performed with HiScript III RT SuperMix for qPCR (Vazyme). The qPCR assays were performed
555 on a QuantStudio 3 Real-Time PCR Systems (Thermo Fisher) using AceQ qPCR SYBR Green Master
556 Mix (Vazyme) according to the manufacturer's protocol. The data were analyzed by QuantStudio (v1.5.2)
557 and visualized by CNSplot (v1.0.1) R package. The expression of genes was normalized to housekeeping
558 gene *GAPDH*, and data were normalized to the mean of the control group. Primer sequences are
559 described in Table S1.

560

561 **Cytokine assays**

562 For each CAR variant, 1×10^5 UTD or CAR-Ms were cocultured with antigen-positive tumor cells in an
563 E/T ratio of 1/1 in complete X-VIVO15 medium and incubated at 37 °C for approximately 24 h. After
564 stimulation, the supernatants were collected and IL-1β, IL-6 or TNFα were measured by ELISA
565 following the manufacturer's protocol (Thermo Fisher).

566

567 **RNA sequencing and data analysis**

568 For bulk RNA-sequencing, K562 and K562-PSMA cells were labeled with green fluorescence using
569 carboxyfluorescein succinimidyl ester (CFSE, Yeasen) method. The hMDMs from independent healthy
570 donors were transduced with the mRNA of indicated CAR variants, and cocultured with either K562 or
571 K562-PSMA cells at a E/T ratio of 1/1 for 24 h. Subsequently, the tumor cells were removed from the
572 cocultures. The absolute removal of tumor cells was confirmed by flow cytometry. Total RNA was

extracted from 5×10^6 CAR-Ms using TRIzol reagent according to the manufacturer's protocol. Next generation sequencing library preparations were conducted according to the manufacturer's protocol. The libraries were sequenced by Novogene on an Illumina NovaSeq X Plus Sequencer. Read quality was assessed with FastQC (v0.12.1) and adapters were trimmed using Cutadapt (v4.4). Reads were then aligned to the GRCh38 genome using HISAT2 (v2.2.1) [51] and reads in exons were counted using featureCounts function in Subread (v2.0.3) package [52]. Analysis of differentially expressed genes was conducted using DESeq2 (v1.40.1) R package. Go analysis was performed using clusterProfiler (v4.10.1) R package [53]. Count data was transformed to log2 scale and normalized with respect to library size using rlog transformation produces. Absolute log2 fold change (log2FC) > 1 and p value < 0.05 was considered statistically significant.

CoSDC library construction using CARode method

The lentiviral vector pLenti6/V5 was used as the backbone vector for CoSDC library construction, because it uses a shorter 3' LTR region, which is suitable for 3' capture kits of scRNA-seq. A codon-optimized gene encoding PSMA CAR composed of CD8α signal peptide, J591 single-chain variable fragments (scFv), CD8α hinge and transmembrane domain was commercially synthesized by GenScript and cloned into the pLenti6/V5 vector. A linker containing XbaI and XhoI restriction sites was insert to C-terminal portion of the CAR construct. ICDs were PCR amplified to combine with first round linkers, a cloning cassette (containing BamHI and XhoI restriction sites) and a unique 6-bp barcode (a linker-cassette-barcode-linker construct). The PSMA CAR vector was digested with FastDigest XbaI (Thermo Fisher) and FastDigest XhoI (Thermo Fisher). The ICDs were individually cloned into the PSMA CAR vector using Gibson Assembly. Then, the bacterial transformation was conducted using the obtained

595 products. The bacteria containing different CAR variant vectors were pooled at equal OD ratios, and
596 lysed to extract G1 library plasmid. The single ICD fragments were PCR amplified again to combine
597 with second round "linker-cassette-barcode-linker". The G1 library was digested with FastDigest BamHI
598 (Thermo Fisher) and FastDigest XhoI (Thermo Fisher). The 2nd ICDs were individually cloned into the
599 G1 to generate G2 library. Similarly, ICDs were PCR amplified to combine with third round "linker-
600 cassette-barcode-linker". The G2 library was digested with BamHI and XhoI enzyme. The 3rd ICDs were
601 individually cloned into the G2 to generate G3 library. The G1, G2 and G3 library and a truncated CAR
602 were pooled together, and digested with FastDigest BcuI (Thermo Fisher). The internal ribosome entry
603 site (IRES) elements and EGFP fluorescence were inserted into the cloning cassette. The products were
604 electroporated into Endura Electrocompetent cells (LGC), and purified to generate the CoSDC plasmid
605 library.
606
607 **Single-cell RNA sequencing and single-cell CAR sequencing**
608 The CoSDC lentiviral library was generated as described above, and transduced to THP-1 cells at a MOI
609 of 0.3 to minimize multiple integrations per cell. The $EGFP^+$ cells were sorted, PMA-induced and
610 cocultured with high PSMA-expressing tumor cell PC3-PSMA at an E/T ratio of 1/1 for 24 h.
611 Immediately after coculture, $EGFP^+$ CAR-Ms were sorted by FACS, and scRNA-seq library was
612 constructed using the 10X Genomics Chromium system following manufacturer's instructions. In brief,
613 the suspended cells were loaded into Chromium microfluidic chips and barcoded with a 10× Chromium
614 Controller (10X Genomics). RNA from the barcoded cells was subsequently reverse-transcribed. The
615 barcoded cDNA was purified and amplified, followed by fragmenting, A-tailing and ligation with
616 adaptors. The 10X scRNA-seq libraries were sequenced by Novogene on an Illumina NovaSeq X Plus

Sequencer. For scCAR-seq, CARode sequences were PCR amplified from 100 ng unfragmented 10X cDNA, and Illumina sequencing adaptors were appended using NEBNext Ultra II Q5 Master Mix (NEB). The CARode libraries were sequenced by Novogene on an Illumina NovaSeq X Plus Sequencer.

For scRNA-seq analysis, raw 10X sequencing reads were aligned to the GRCh38 genome using Cell Ranger (v7.2.0). Gene expression profiles were processed using Seurat (v5.1.0) R package [54]. Briefly, quality control was applied to cells based on the total UMI counts and number of detected genes. Cells with less than 5,000 UMI count were filtered, as well as cells with more than 10% mitochondrial gene count. To remove potential doublets, cells with UMI count above 70,000 and detected genes above 9,000 are filtered out. The gene counts were normalized using SCTransform. For clustering, top 2,000 variable genes were used, and ribosomal and mitochondrial genes were removed from the variable gene set before running PCA and identifying clusters using a shared nearest neighbor (SNN) modularity optimization-based clustering algorithm. The Seurat normalized count matrix was used for the downstream analysis.

For scCAR-seq analysis, the CARode sequences for each cell were extracted from the raw sequencing reads and mapped to signal domains. A total of over 21 million CARode reads were obtained from 16,612 single cells. Cells with more than 10 CARode reads were classified as CAR-Ms. 7911 cells expressing a single specific CAR variant were identified from the scRNA-seq data for subsequent clustering and functional analyses.

Gene set activity analysis

AUCell (v1.24.0) R package [55] was employed to assess the gene set activities in scRNA-seq data. AUCell uses the “Area Under the Curve” (AUC) score to quantify the expression level of an input gene

set for each cell. Previously established M1 and M2 signatures [56] were used for macrophage polarization analysis. MacSpectrum (v0.1.0) R package [57] was also employed to assess macrophage activation. To evaluate antigen processing and presentation, gene sets from the Reactome (2132295, 983169), KEGG (04612), and GO (0019882) databases were used. Additionally, KEGG (04666) and GO (0006909) gene sets were used to estimate phagocytic activity. MMP family genes MMP1-28 were applied to analyze MMP expression levels.

Cytotoxicity assay

To measure specific killing, a bioluminescence (BLI)-based cytotoxicity assay was performed. FFluc-positive PC3-PSMA, SKOV3, and HepG2 tumor cells were used as targets. CAR-Ms were cocultured with 10,000 target cells at the specified E/T ratios in complete X-VIVO15 medium on black 96-well flat-bottom plates. The BLI was measured using a luminometer (Tecan Spark) in relative light units (RLU). A spontaneous death control was used including tumor cells alone. The maximal death control contained 1% Triton X-100 and tumor cells. Specific lysis was calculated using: %Specific Lysis = 100 × (average spontaneous death RLU − test RLU)/(average spontaneous death RLU − average maximal death RLU). Negative specific lysis values indicate more signal than in the spontaneous death control wells.

Statistical analysis

Statistical analysis was performed using rstatix (v0.7.2) R package. Statistical details for all experiments can be found in the figure legends. Error bars indicated the Standard Error of Mean (s.e.m.). Differences were analyzed by unpaired Student's t test or one-way ANOVA depending on experimental conditions.

Unless otherwise indicated, the experiments were performed independently in triplicate, and n is indicated in the figure legends.

Acknowledgements

Thanks to members of Shen's laboratory for helpful discussions, technical assistance, and critical reading of the manuscript. We thank Fuchou Tang and Lu Wen from Peking University, and Jiaming Su from Zhejiang University for their help in library construction, high-throughput sequencing and lentiviral transduction. This work was supported by grants from the Natural Science Foundation of Jiangsu Province (BK20222009 to P. Shen), the Pivotal Life Sciences Sponsorship Program (1352806 to P. Shen), the Program from National Center of Technology Innovation for Biopharmaceuticals (NCTIB2023XB01013 to P. Shen), the Program from Proof of Concept Center of Jiangsu Province (Research, Development and Clinical Study of Chimeric Antigen Receptor Macrophage Immunotherapy Technology Targeting Malignant Prostate Cancer), and the Guangdong Basic and Applied Basic Research Foundation (2021B1515120016 to P. Shen).

Author contributions

Y. Wang and S. Zuo conceived the project and performed experiments and data analysis. H. Bao, Z. Zhang, and Q. Liu performed experiments. Y. Chen, W. Zhang, Y. Lu, Y. Huang, W. Zheng, N. Yang, and L. Ye provided scientific suggestions and contributed to the manuscript revision. P. Shen supervised the project and wrote the manuscript. The author(s) read and approved the final manuscript.

Data availability

683 RNA-seq, scRNA-seq, scCAR-seq data have been deposited in the Gene Expression Omnibus repository
684 under accession code GSE289202.
685
686 **References**

687 1. June, C.H., et al., *CAR T cell immunotherapy for human cancer.* Science, 2018. **359**(6382):
688 p. 1361-1365.
689 2. Cappell, K.M. and J.N. Kochenderfer, *Long-term outcomes following CAR T cell therapy:*
690 *what we know so far.* Nat Rev Clin Oncol, 2023. **20**(6): p. 359-371.
691 3. Maalej, K.M., et al., *CAR-cell therapy in the era of solid tumor treatment: current*
692 *challenges and emerging therapeutic advances.* Mol Cancer, 2023. **22**(1): p. 20.
693 4. Newick, K., et al., *CAR T Cell Therapy for Solid Tumors.* Annu Rev Med, 2017. **68**: p. 139-
694 152.
695 5. Mantovani, A., et al., *Macrophages as tools and targets in cancer therapy.* Nat Rev Drug
696 Discov, 2022. **21**(11): p. 799-820.
697 6. Reiss, K.A., et al., *CAR-macrophage therapy for HER2-overexpressing advanced solid*
698 *tumors: a phase 1 trial.* Nat Med, 2025.
699 7. Christofides, A., et al., *The complex role of tumor-infiltrating macrophages.* Nat Immunol,
700 2022. **23**(8): p. 1148-1156.
701 8. Cassetta, L. and J.W. Pollard, *A timeline of tumour-associated macrophage biology.* Nat
702 Rev Cancer, 2023. **23**(4): p. 238-257.
703 9. Zhang, W., et al., *Chimeric antigen receptor macrophage therapy for breast tumours*
704 *mediated by targeting the tumour extracellular matrix.* Br J Cancer, 2019. **121**(10): p. 837-

845.

10. Klichinsky, M., et al., *Human chimeric antigen receptor macrophages for cancer immunotherapy.* Nat Biotechnol, 2020. **38**(8): p. 947-953.

11. Lei, A., et al., *A second-generation M1-polarized CAR macrophage with antitumor efficacy.* Nat Immunol, 2024. **25**(1): p. 102-116.

12. Sloas, C., S. Gill, and M. Klichinsky, *Engineered CAR-Macrophages as Adoptive Immunotherapies for Solid Tumors.* Front Immunol, 2021. **12**: p. 783305.

13. Dong, X., et al., *Efficacy evaluation of chimeric antigen receptor-modified human peritoneal macrophages in the treatment of gastric cancer.* Br J Cancer, 2023. **129**(3): p. 551-562.

14. Morrissey, M.A., et al., *Chimeric antigen receptors that trigger phagocytosis.* Elife, 2018. **7**.

15. Shah, Z., et al., *Human anti-PSCA CAR macrophages possess potent antitumor activity against pancreatic cancer.* Cell Stem Cell, 2024. **31**(6): p. 803-817 e6.

16. Duan, Z., et al., *Chimeric antigen receptor macrophages activated through TLR4 or IFN-gamma receptors suppress breast cancer growth by targeting VEGFR2.* Cancer Immunol Immunother, 2023. **72**(10): p. 3243-3257.

17. Dong, M.B., et al., *Tumor immunology CRISPR screening: present, past, and future.* Trends Cancer, 2022. **8**(3): p. 210-225.

18. Gordon, K.S., et al., *Screening for CD19-specific chimaeric antigen receptors with enhanced signalling via a barcoded library of intracellular domains.* Nat Biomed Eng, 2022. **6**(7): p. 855-866.

19. Castellanos-Rueda, R., et al., *speedingCARs: accelerating the engineering of CAR T cells*

727 *by signaling domain shuffling and single-cell sequencing.* Nat Commun, 2022. **13**(1): p.
728 6555.
729 20. Blaeschke, F., et al., *Modular pooled discovery of synthetic knockin sequences to program*
730 *durable cell therapies.* Cell, 2023. **186**(19): p. 4216-4234 e33.
731 21. Daniels, K.G., et al., *Decoding CAR T cell phenotype using combinatorial signaling motif*
732 *libraries and machine learning.* Science, 2022. **378**(6625): p. 1194-1200.
733 22. Goodman, D.B., et al., *Pooled screening of CAR T cells identifies diverse immune signaling*
734 *domains for next-generation immunotherapies.* Science Translational Medicine, 2022.
735 **14**(670): p. eabm1463.
736 23. Ginhoux, F. and S. Jung, *Monocytes and macrophages: developmental pathways and*
737 *tissue homeostasis.* Nat Rev Immunol, 2014. **14**(6): p. 392-404.
738 24. Ferreira, I., et al., *Cell Cycle Regulation in Macrophages and Susceptibility to HIV-1.* Viruses,
739 2020. **12**(8).
740 25. Lindner, B., et al., *A genome-wide CRISPR/Cas9 screen to identify phagocytosis*
741 *modulators in monocytic THP-1 cells.* Sci Rep, 2021. **11**(1): p. 12973.
742 26. Luteijn, R.D., et al., *SLC19A1 transports immunoreactive cyclic dinucleotides.* Nature, 2019.
743 **573**(7774): p. 434-438.
744 27. Sack, L.M., et al., *Profound Tissue Specificity in Proliferation Control Underlies Cancer*
745 *Drivers and Aneuploidy Patterns.* Cell, 2018. **173**(2): p. 499-514 e23.
746 28. Garcia, J., et al., *Naturally occurring T cell mutations enhance engineered T cell therapies.*
747 Nature, 2024. **626**(7999): p. 626-634.
748 29. Lanier, L.L., *DAP10- and DAP12-associated receptors in innate immunity.* Immunol Rev,

749 2009. **227**(1): p. 150-60.

750 30. Washington, A.V., et al., *TREM-like transcript-1 protects against inflammation-associated*
751 *hemorrhage by facilitating platelet aggregation in mice and humans.* J Clin Invest, 2009.
752 **119**(6): p. 1489-501.

753 31. Chen, L. and D.B. Flies, *Molecular mechanisms of T cell co-stimulation and co-inhibition.*
754 Nat Rev Immunol, 2013. **13**(4): p. 227-42.

755 32. Kaur, G., J. Trowsdale, and L. Fugger, *Natural killer cells and their receptors in multiple*
756 *sclerosis.* Brain, 2013. **136**(Pt 9): p. 2657-76.

757 33. Labanieh, L., R.G. Majzner, and C.L. Mackall, *Programming CAR-T cells to kill cancer.* Nat
758 Biomed Eng, 2018. **2**(6): p. 377-391.

759 34. Mellman, I., et al., *The cancer-immunity cycle: Indication, genotype, and immunotype.*
760 Immunity, 2023. **56**(10): p. 2188-2205.

761 35. Zhang, J., et al., *Turning cold tumors hot: from molecular mechanisms to clinical*
762 *applications.* Trends Immunol, 2022. **43**(7): p. 523-545.

763 36. Dougan, M., G. Dranoff, and S.K. Dougan, *GM-CSF, IL-3, and IL-5 Family of Cytokines:*
764 *Regulators of Inflammation.* Immunity, 2019. **50**(4): p. 796-811.

765 37. Spangler, J.B., et al., *Insights into cytokine-receptor interactions from cytokine*
766 *engineering.* Annu Rev Immunol, 2015. **33**: p. 139-67.

767 38. Brandsma, A.M., et al., *Fc receptor inside-out signaling and possible impact on antibody*
768 *therapy.* Immunol Rev, 2015. **268**(1): p. 74-87.

769 39. Xue, J., et al., *Transcriptome-based network analysis reveals a spectrum model of human*
770 *macrophage activation.* Immunity, 2014. **40**(2): p. 274-88.

771 40. Pizzurro, G.A. and K. Miller-Jensen, *Reframing macrophage diversity with network motifs.*
772 Trends Immunol, 2023. **44**(12): p. 965-970.
773 41. Locati, M., G. Curtale, and A. Mantovani, *Diversity, Mechanisms, and Significance of*
774 *Macrophage Plasticity.* Annu Rev Pathol, 2020. **15**: p. 123-147.
775 42. Laguette, N., et al., *SAMHD1 is the dendritic- and myeloid-cell-specific HIV-1 restriction*
776 *factor counteracted by Vpx.* Nature, 2011. **474**(7353): p. 654-7.
777 43. Berger, A., et al., *SAMHD1-deficient CD14+ cells from individuals with Aicardi-Goutieres*
778 *syndrome are highly susceptible to HIV-1 infection.* PLoS Pathog, 2011. **7**(12): p.
779 e1002425.
780 44. Hrecka, K., et al., *Vpx relieves inhibition of HIV-1 infection of macrophages mediated by*
781 *the SAMHD1 protein.* Nature, 2011. **474**(7353): p. 658-61.
782 45. Haney, M.S., et al., *Identification of phagocytosis regulators using magnetic genome-wide*
783 *CRISPR screens.* Nat Genet, 2018. **50**(12): p. 1716-1727.
784 46. Tedesco, S., et al., *Convenience versus Biological Significance: Are PMA-Differentiated*
785 *THP-1 Cells a Reliable Substitute for Blood-Derived Macrophages When Studying in Vitro*
786 *Polarization?* Front Pharmacol, 2018. **9**: p. 71.
787 47. Mohd Yasin, Z.N., et al., *Macrophage polarization in THP-1 cell line and primary*
788 *monocytes: A systematic review.* Differentiation, 2022. **128**: p. 67-82.
789 48. Love, M.I., W. Huber, and S. Anders, *Moderated estimation of fold change and dispersion*
790 *for RNA-seq data with DESeq2.* Genome Biol, 2014. **15**(12): p. 550.
791 49. Kolde, R., et al., *Robust rank aggregation for gene list integration and meta-analysis.*
792 Bioinformatics, 2012. **28**(4): p. 573-80.

50. Subach, O.M., et al., *An enhanced monomeric blue fluorescent protein with the high chemical stability of the chromophore.* PLoS One, 2011. **6**(12): p. e28674.

51. Kim, D., et al., *Graph-based genome alignment and genotyping with HISAT2 and HISAT-genotype.* Nat Biotechnol, 2019. **37**(8): p. 907-915.

52. Liao, Y., G.K. Smyth, and W. Shi, *featureCounts: an efficient general purpose program for assigning sequence reads to genomic features.* Bioinformatics, 2014. **30**(7): p. 923-30.

53. Wu, T., et al., *clusterProfiler 4.0: A universal enrichment tool for interpreting omics data.* Innovation (Camb), 2021. **2**(3): p. 100141.

54. Hao, Y., et al., *Dictionary learning for integrative, multimodal and scalable single-cell analysis.* Nat Biotechnol, 2024. **42**(2): p. 293-304.

55. Aibar, S., et al., *SCENIC: single-cell regulatory network inference and clustering.* Nat Methods, 2017. **14**(11): p. 1083-1086.

56. Martinez, F.O., et al., *Transcriptional profiling of the human monocyte-to-macrophage differentiation and polarization: new molecules and patterns of gene expression.* J Immunol, 2006. **177**(10): p. 7303-11.

57. Li, C., et al., *Single cell transcriptomics based-MacSpectrum reveals novel macrophage activation signatures in diseases.* JCI Insight, 2019. **5**(10).

Competing interests

The Shen lab has received research support from Macera therapeutics. P. Shen is a compensated co-founder, member of the scientific advisory board, and works as the CSO of Macera therapeutics. Y. Chen

815 is a compensated co-founder, and works as the CEO of Macera therapeutics. W. Zhang works as the
816 Process Development Director of Macera therapeutics. P. Shen, Y. Wang, S. Zuo, Y. Chen, and W. Zhang
817 are listed on patent applications related to this work. The other authors declare no competing interests.
818

819 **Figure legends**

820 **Figure 1. NaSDC×CoSDC screens identify therapeutic CAR-M candidates**

821 **(A)** Schematic illustration of the NaSDC×CoSDC platform.

822 **(B)** Flow cytometric histograms showing EGFP expression in hMDMs and THP-1 cells transduced with
823 an EGFP reporter lentivirus. Grey peaks indicate protein expression levels in untransduced (UTD) cells.

824 **(C)** Flow cytometric plots illustrating the NaSDC library sorting strategy (left) and CAR expression
825 levels (right).

826 **(D)** Schematic representation of the CoSDC library and CARode. ICD, intracellular domain.

827 Data in (**B)** and (**C)** are representative of three independent experiments.
828

829 **Figure 2. NaSDC screens reveal known and novel CAR-M candidates**

830 **(A)** Schematic representation of the pro-phagocytic module screening strategy.

831 **(B)** Correlation between log2 fold change and −log10 rho scores for pro-phagocytic CAR variant screens.
832 Data represent 18 biological replicates across six NaSDC lentivirus batches.

833 **(C)** FACS-based quantification of PC3-PSMA tumor cell phagocytosis by CAR-Ms (n = 4 biological
834 replicates).

835 **(D)** Schematic representation of the pro-inflammatory module screening strategy.

836 **(E)** Correlation between log2 fold change and −log10 rho scores for pro-inflammatory CAR variant

screens. Data represent 15 biological replicates across five NaSDC lentivirus batches.

(F) Relative mRNA expression of *TNF*, *IL6* and *IL1B* in CAR-Ms cocultured with PSMA positive target tumor cells (n = 4 biological replicates).

(G) Schematic representation of the pro-infiltrating module screening strategy.

(H) Correlation between log2 fold change and −log10 rho scores for pro-infiltrating CAR variant screens. Data represent 9 biological replicates across three NaSDC lentivirus batches.

(I) Relative mRNA expression of MMP family genes in CAR-Ms cocultured with PSMA positive target tumor cells (n = 4 biological replicates).

Dashed lines in (**C**, **F**, **I**) indicate −log10(0.05) (horizontal) and log2 fold change of truncated CARs (CARΔ) (vertical). Data in (C) are presented as mean ± s.e.m. and analyzed using one-way ANOVA followed by Dunnett's multiple-comparison test.

Figure 3. CoSDC screens identify CAR signaling combinations that enhance macrophage anti-tumor functions

(A) Schematic illustration of the CoSDC library and scCAR-seq screening platform.

(B) Proportion of cells expressing different numbers of CAR variants (left), and tSNE-based dimensionality reduction and clustering (right) for single-CAR-expressing cells (right).

(C) MacSpectrum plot showing macrophage polarization states of single-cell clusters. MPI, macrophage polarization index. AMDI, activation-induced macrophage differentiation index. Data are represented as means of clusters. Black dashed line represents the mean MPI of CARΔ.

(D) Feature plots showing the distribution of AUC scores for antigen processing and presentation-related gene sets. Reactome gene sets "MHC class II antigen presentation" (2132295) and "Class I MHC

859 mediated antigen processing & presentation" (983169), GO gene sets "Antigen processing and
860 presentation" (0019882), and KEGG pathway "Antigen processing and presentation" (04612) were used.
861 **(E)** Normalized AUC scores for MMP-related genes. Dashed line indicates the mean AUC score of
862 CARΔ.
863 **(F)** Dot plot showing the phagocytosis scores for single-cell clusters. KEGG pathway "Fc gamma R-
864 mediated phagocytosis" (04666) and GO gene set "Phagocytosis" (0006909) were used.
865 **(G)** Heatmap showing log2 fold change (c0 vs the other clusters) of each ICD in third-generation CARs.
866
867 **Figure 4. Combinatorial CAR constructs enhance macrophage phagocytosis, pro-inflammatory**
868 **activation, and infiltration capacity**
869 **(A)** Description of CAR variants used for individual characterization.
870 **(B)** FACS-based quantification of PC3-PSMA tumor cell phagocytosis by UTD and CAR-Ms (n = 4
871 biological replicates).
872 **(C)** Flow cytometric histograms showing surface expression of CD80 and CD86 in UTD and CAR-Ms
873 cocultured with PSMA positive tumor cells.
874 **(D)** Flow cytometric histograms of reactive oxygen species (ROS) levels in UTD and CAR-Ms
875 cocultured with PSMA positive tumor cells. DCF, 2'-7'dichlorofluorescein.
876 **(E)** Relative mRNA expression of *TNF* and *IL6* in UTD and CAR-Ms cocultured with PSMA positive
877 tumor cells (n = 4 biological replicates).
878 **(F)** Relative mRNA expression of *MMP11* and *MMP13* in UTD and CAR-Ms cocultured with PSMA
879 positive tumor cells (n = 4 biological replicates).
880 Data in (**B**) are presented as mean ± s.e.m. and analyzed using one-way ANOVA followed by Dunnett's

881 multiple-comparison. Data in (**C**, **D)** are representative of three independent experiments. Dashed lines

882 (**C**, **D**) represent the mean fluorescence intensity (MFI) for UTD macrophages.

883

884 **Figure 5. CD40-LY9-FCRL1 CAR-Ms reshape the TME**

885 **(A)** Schematic illustration of the humanized immune system TME model. PC3-PSMA tumors were

886 established bilaterally, followed by PBMC engraftment on day 7. On day 14, 5×10^6 UTD or CAR-Ms

887 were injected IT. Tumors were harvested on day 18 for scRNA-seq. SC, subcutaneously. IV,

888 intravenously. IT, intratumorally.

889 **(B)** Proportions of cell types from scRNA-seq (left) and tSNE-based clustering of all sequenced cells

890 (right). B, B cell. T, T cell. Mac, macrophage.

891 **(C)** Dimensionality reduction (tSNE) and clustering for macrophages. Data are colored by treatment

892 conditions.

893 **(D)** Density plots within tSNE maps depicting the distribution of CAR-expressing cells.

894 **(E)** AUC scores of M1 and M2 gene sets in the indicated macrophage clusters.

895 **(F)** Feature plots showing expression levels of selected genes.

896 **(G)** MFI of HLA-ABC and HLA-DR in UTD and CAR-Ms after 24 h coculture with PSMA positive

897 tumor cells (n = 3 biological replicates).

898 **(H)** AUC scores of T cell cytotoxicity and exhaustion gene sets in the indicated T cell clusters.

899 Unless specified otherwise, data are presented as mean ± s.e.m. and analyzed using the two-tailed

900 Student's t-test.

901

902 **Figure 6. CD40-LY9-FCRL1 CAR-Ms improve solid tumor clearance *in vitro* and *in vivo***

903 **(A)** Specific killing of PC3-PSMA cells by UTD and COMB7 CAR-Ms at varying E/T ratios. Data

904 represent two independent experiments from two human donors.

905 **(B)** Specific killing of PC3-PSMA cells by UTD, CD247 CAR-Ms or COMB7 CAR-Ms at an E/T ratio

906 of 3/1. Data collected from two human donors.

907 **(C-D)** Specific killing of $HER2^+$ SKOV3 or $GPC3^+$ HepG2 cells by UTD or COMB7 CAR-Ms at an E/T

908 ratio of 3/1 (n = 6 biological replicates).

909 **(E)** NCG mice were IP injected with 1×10^6 PC3-PSMA cells, followed by treatment with PBS, 5×10^6

910 UTD, or 5×10^6 COMB7 CAR-Ms one day later.

911 **(F)** Overall survival for mice in each treatment group (n = 6 for PBS, n = 5 for UTD and COMB7).

912 **(G)** Tumor burden measured by bioluminescence (total flux). Data shown are individual values (n = 6

913 for PBS, n = 5 for UTD and COMB7).

914 Unless specified otherwise, data are presented as mean ± s.e.m. and analyzed using the two-tailed

915 Student's t-test.

916

Figure1

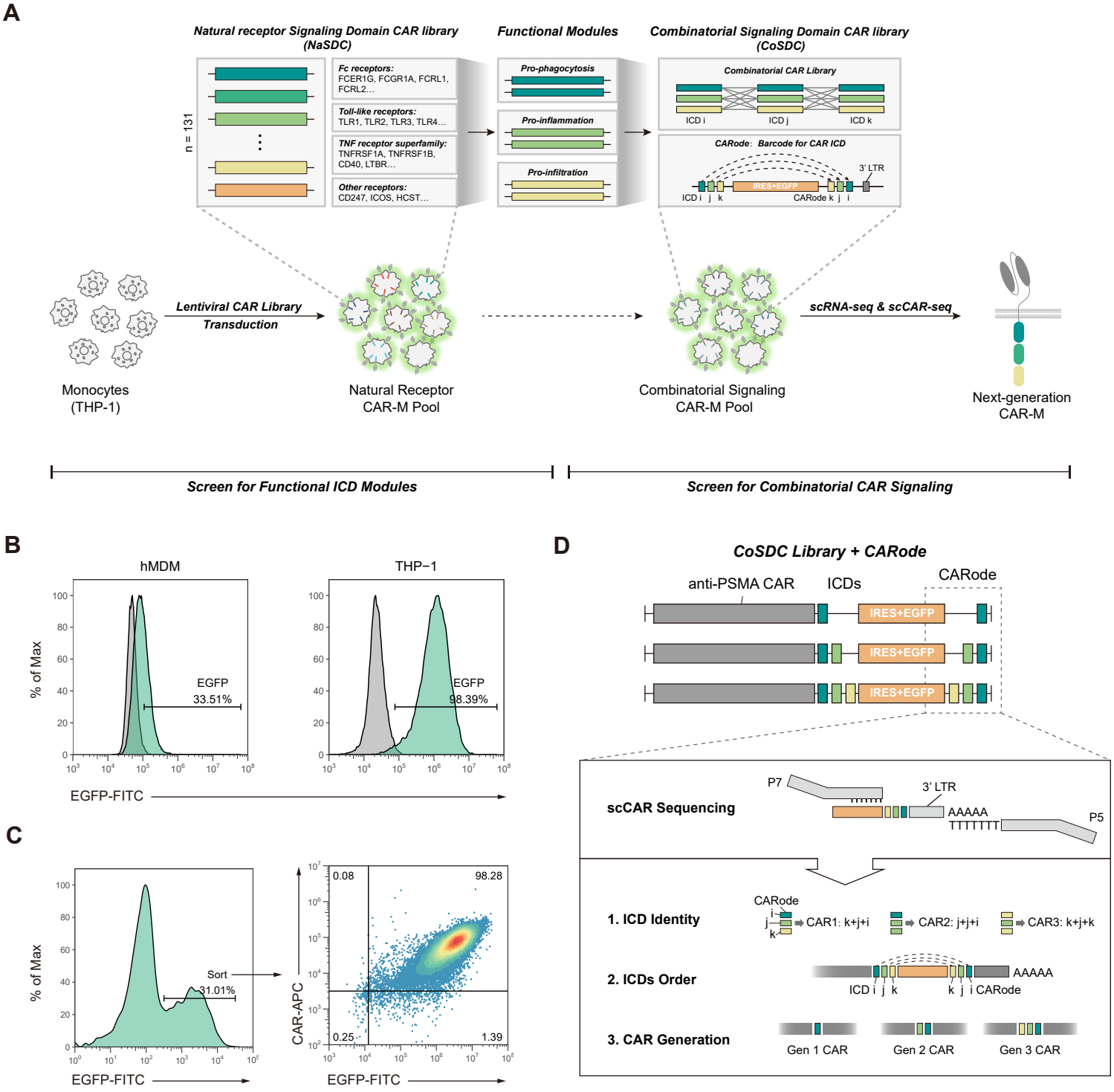
A
Natural receptor Signaling Domain CAR library (NaSDC)
Functional Modules
Combinatorial Signaling Domain CAR library (CoSDC)
n = 131
Fc receptors: FCER1G, FCGR1A, FCRL1, FCRL2…
Toll-like receptors: TLR1, TLR2, TLR3, TLR4…
TNF receptor superfamily: TNFRSF1A, TNFRSF1B, CD40, LTBR…
Other receptors: CD247, ICOS, HCST…
Pro-phagocytosis
Pro-inflammation
Pro-infiltration
Combinatorial CAR Library
ICD i
ICD j
ICD k
CARode: Barcode for CAR ICD
3' LTR
IRES+EGFP
ICD i j k
CARode k j i
Lentiviral CAR Library Transduction
scRNA-seq & scCAR-seq
Monocytes (THP-1)
Natural Receptor CAR-M Pool
Combinatorial Signaling CAR-M Pool
Next-generation CAR-M
Screen for Functional ICD Modules
Screen for Combinatorial CAR Signaling
B
hMDM
THP−1
% of Max
EGFP 33.51%
EGFP 98.39%
EGFP-FITC
C
% of Max
Sort
31.01%
EGFP-FITC
CAR-APC
0.08
98.28
0.25
1.39
EGFP-FITC
D
CoSDC Library + CARode
anti-PSMA CAR
ICDs
CARode
IRES+EGFP
scCAR Sequencing
P7
3' LTR
AAAAA
TTTTTTT
P5
1. ICD Identity
CARode
CAR1: k+j+i
CAR2: j+j+i
CAR3: k+j+k
2. ICDs Order
AAAAA
ICD i j k
k j i CARode
3. CAR Generation
Gen 1 CAR
Gen 2 CAR
Gen 3 CAR

Figure2

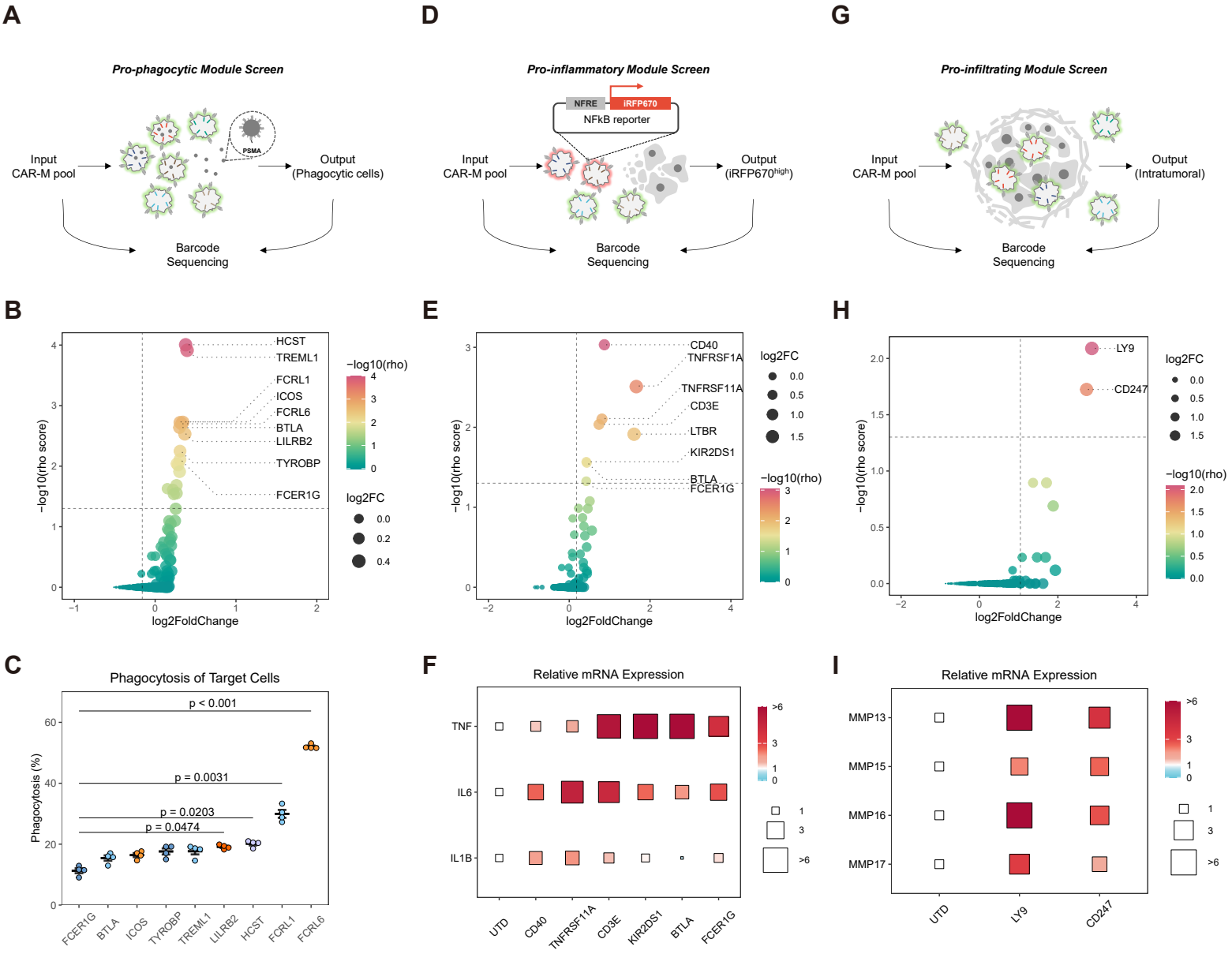
A
Pro-phagocytic Module Screen
Input
CAR-M pool
PSMA
Output
(Phagocytic cells)
Barcode
Sequencing
D
Pro-inflammatory Module Screen
NFRE
iRFP670
NFkB reporter
Input
CAR-M pool
Output
(iRFP670high)
Barcode
Sequencing
G
Pro-infiltrating Module Screen
Input
CAR-M pool
Output
(Intratumoral)
Barcode
Sequencing
B
HCST
TREML1
FCRL1
ICOS
FCRL6
BTLA
LILRB2
TYROBP
FCER1G
−log10(rho)
log2FC
−log10(rho score)
log2FoldChange
E
CD40
TNFRSF1A
TNFRSF11A
CD3E
LTBR
KIR2DS1
BTLA
FCER1G
log2FC
−log10(rho)
−log10(rho score)
log2FoldChange
H
LY9
CD247
log2FC
−log10(rho)
−log10(rho score)
log2FoldChange
C
Phagocytosis of Target Cells
p < 0.001
p = 0.0031
p = 0.0203
p = 0.0474
Phagocytosis (%)
FCER1G
BTLA
ICOS
TYROBP
TREML1
LILRB2
HCST
FCRL1
FCRL6
F
Relative mRNA Expression
TNF
IL6
IL1B
UTD
CD40
TNFRSF11A
CD3E
KIR2DS1
BTLA
FCER1G
I
Relative mRNA Expression
MMP13
MMP15
MMP16
MMP17
UTD
LY9
CD247

Figure3

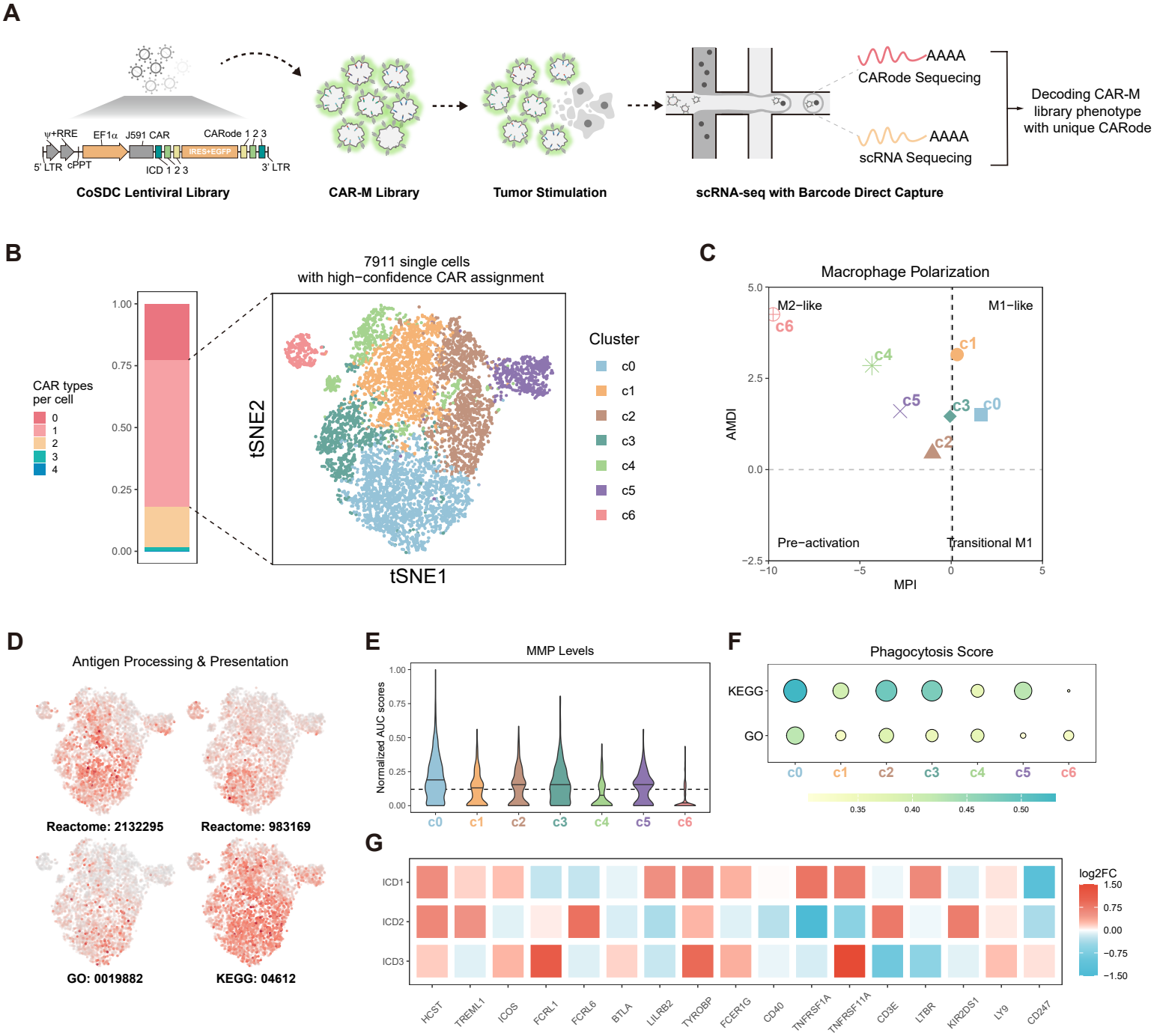
A
ψ+RRE
EF1α
J591 CAR
CARode 1 2 3
IRES+EGFP
5' LTR
cPPT
ICD 1 2 3
3' LTR
CoSDC Lentiviral Library
CAR-M Library
Tumor Stimulation
scRNA-seq with Barcode Direct Capture
AAAA
CARode Sequecing
AAAA
scRNA Sequecing
Decoding CAR-M library phenotype with unique CARode
B
7911 single cells
with high−confidence CAR assignment
CAR types per cell
0
1
2
3
4
tSNE2
tSNE1
Cluster
c0
c1
c2
c3
c4
c5
c6
C
Macrophage Polarization
M2−like
M1−like
Pre−activation
Transitional M1
AMDI
MPI
D
Antigen Processing & Presentation
Reactome: 2132295
Reactome: 983169
GO: 0019882
KEGG: 04612
E
MMP Levels
Normalized AUC scores
F
Phagocytosis Score
KEGG
GO
G
ICD1
ICD2
ICD3
HCST
TREML1
ICOS
FCRL1
FCRL6
BTLA
LILRB2
TYROBP
FCER1G
CD40
TNFRSF1A
TNFRSF11A
CD3E
LTBR
KIR2DS1
LY9
CD247
log2FC

Figure4

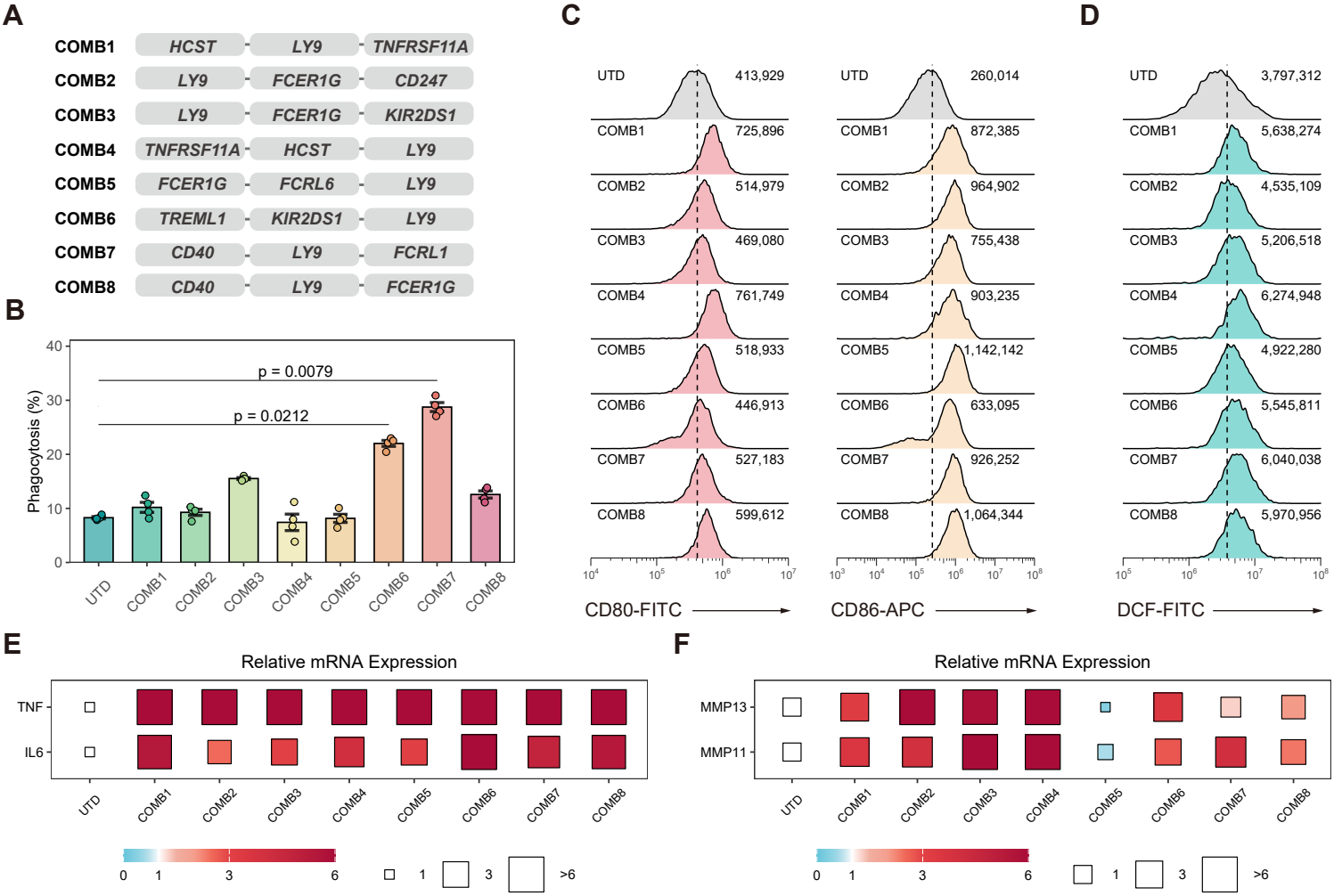
A
COMB1 HCST - LY9 - TNFRSF11A
COMB2 LY9 - FCER1G - CD247
COMB3 LY9 - FCER1G - KIR2DS1
COMB4 TNFRSF11A - HCST - LY9
COMB5 FCER1G - FCRL6 - LY9
COMB6 TREML1 - KIR2DS1 - LY9
COMB7 CD40 - LY9 - FCRL1
COMB8 CD40 - LY9 - FCER1G
B
Phagocytosis (%)
p = 0.0079
p = 0.0212
UTD COMB1 COMB2 COMB3 COMB4 COMB5 COMB6 COMB7 COMB8
C
UTD 413,929
COMB1 725,896
COMB2 514,979
COMB3 469,080
COMB4 761,749
COMB5 518,933
COMB6 446,913
COMB7 527,183
COMB8 599,612
CD80-FITC
UTD 260,014
COMB1 872,385
COMB2 964,902
COMB3 755,438
COMB4 903,235
COMB5 1,142,142
COMB6 633,095
COMB7 926,252
COMB8 1,064,344
CD86-APC
D
UTD 3,797,312
COMB1 5,638,274
COMB2 4,535,109
COMB3 5,206,518
COMB4 6,274,948
COMB5 4,922,280
COMB6 5,545,811
COMB7 6,040,038
COMB8 5,970,956
DCF-FITC
E
Relative mRNA Expression
TNF
IL6
UTD COMB1 COMB2 COMB3 COMB4 COMB5 COMB6 COMB7 COMB8
0 1 3 6
1 3 >6
F
Relative mRNA Expression
MMP13
MMP11
UTD COMB1 COMB2 COMB3 COMB4 COMB5 COMB6 COMB7 COMB8
0 1 3 6
1 3 >6

Figure5

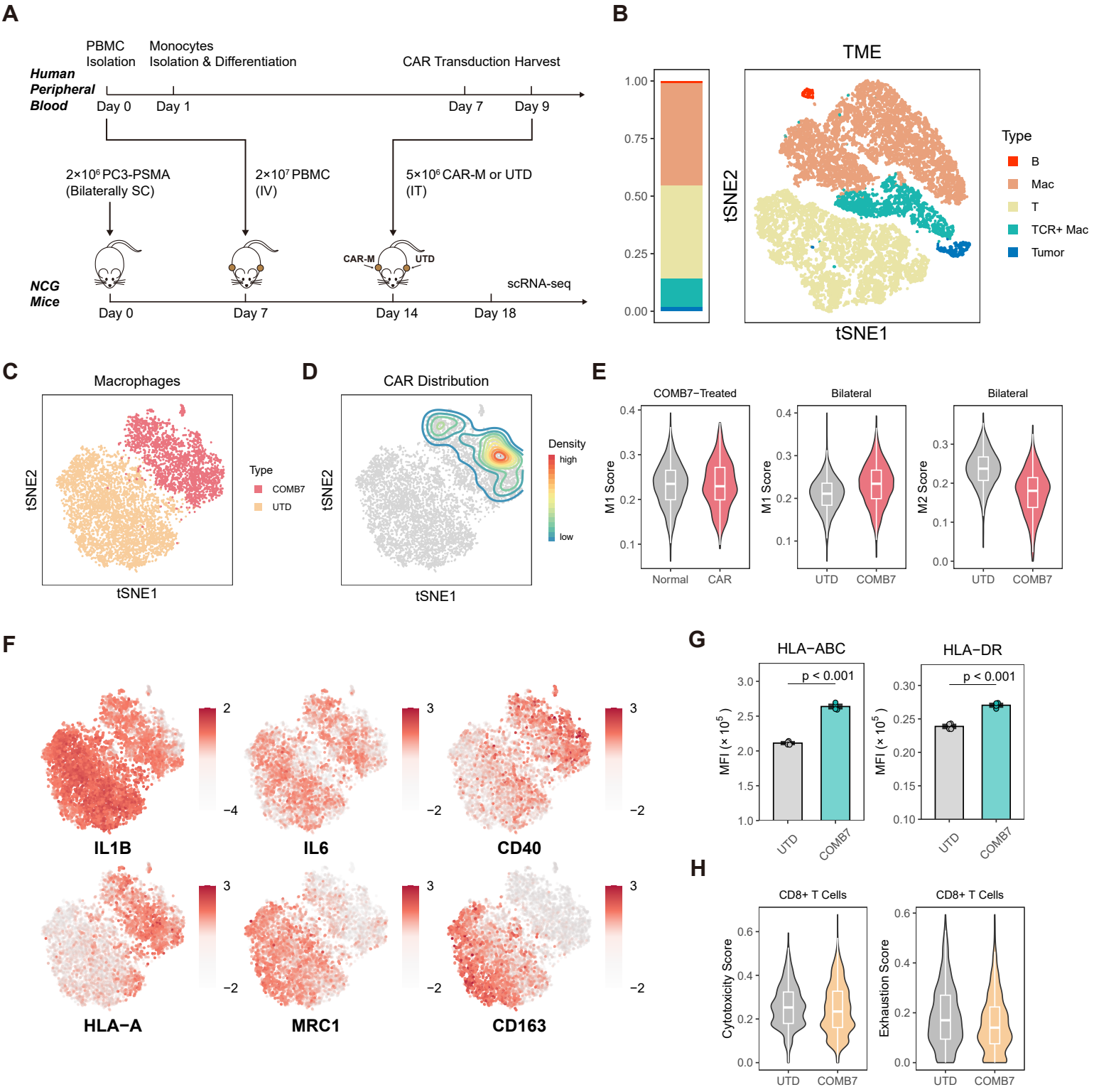
A
PBMC Isolation
Monocytes Isolation & Differentiation
CAR Transduction Harvest
Human Peripheral Blood
Day 0
Day 1
Day 7
Day 9
2×10⁶ PC3-PSMA (Bilaterally SC)
2×10⁷ PBMC (IV)
5×10⁶ CAR-M or UTD (IT)
CAR-M
UTD
NCG Mice
scRNA-seq
Day 0
Day 7
Day 14
Day 18
B
TME
tSNE2
tSNE1
Type
B
Mac
T
TCR+ Mac
Tumor
C
Macrophages
tSNE2
tSNE1
Type
COMB7
UTD
D
CAR Distribution
tSNE2
tSNE1
Density
high
low
E
COMB7−Treated
Bilateral
Bilateral
M1 Score
M1 Score
M2 Score
Normal
CAR
UTD
COMB7
UTD
COMB7
F
IL1B
IL6
CD40
HLA−A
MRC1
CD163
G
HLA−ABC
HLA−DR
p < 0.001
p < 0.001
MFI (× 10⁵)
UTD
COMB7
H
CD8+ T Cells
CD8+ T Cells
Cytotoxicity Score
Exhaustion Score
UTD
COMB7

Figure6

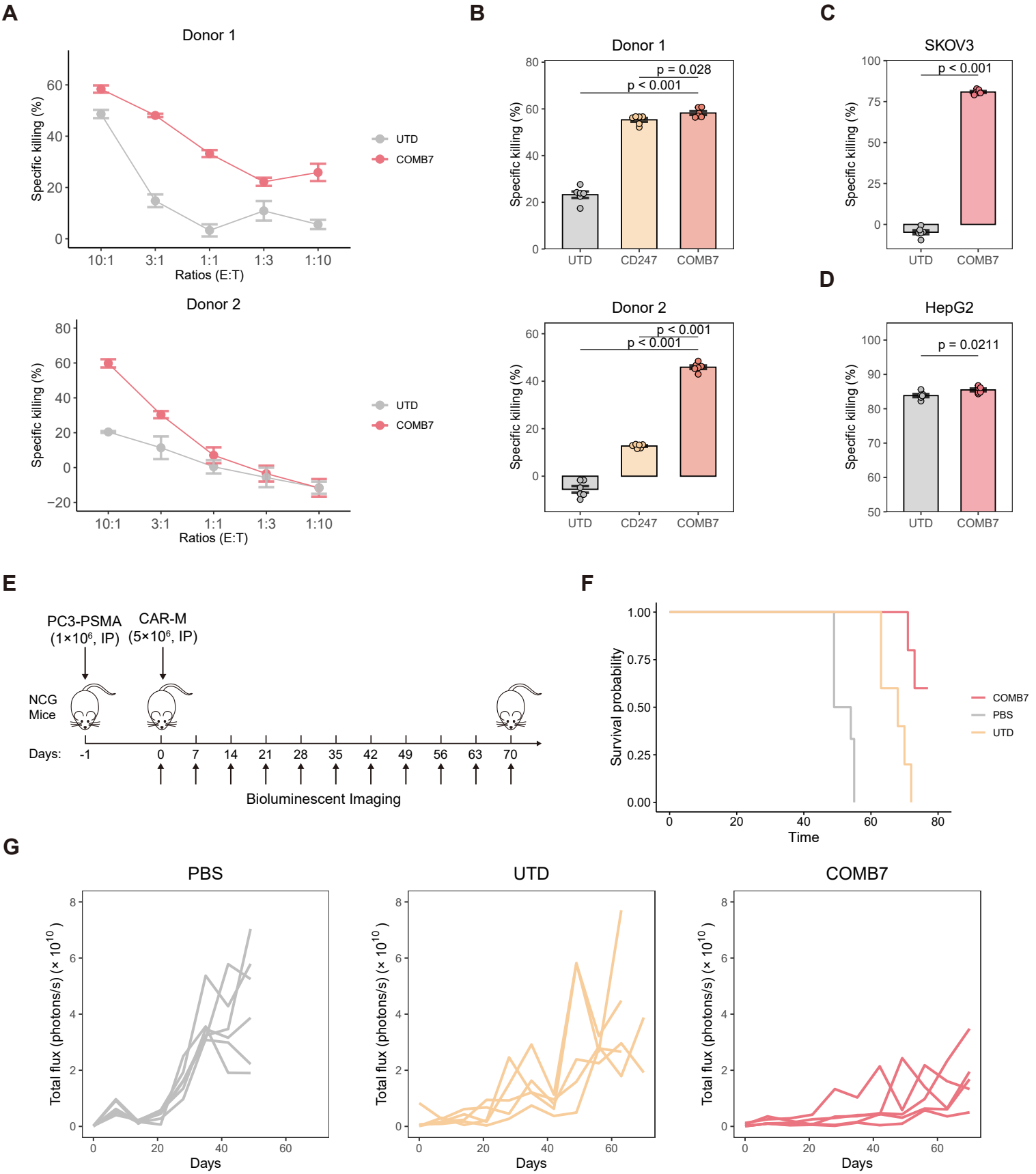
A
Donor 1
Specific killing (%)
Ratios (E:T)
10:1
3:1
1:1
1:3
1:10
UTD
COMB7
Donor 2
B
Donor 1
p = 0.028
p < 0.001
UTD
CD247
COMB7
Donor 2
p < 0.001
p < 0.001
C
SKOV3
p < 0.001
D
HepG2
p = 0.0211
E
PC3-PSMA
(1×10⁶, IP)
CAR-M
(5×10⁶, IP)
NCG
Mice
Days:
-1
0
7
14
21
28
35
42
49
56
63
70
Bioluminescent Imaging
F
Survival probability
Time
COMB7
PBS
UTD
G
PBS
UTD
COMB7
Total flux (photons/s) (× 10¹⁰)
Days